CoA Note No.92

THE COLLEGE OF AERONAUTICS

CRANFIELD

EFFECT OF BODY INCIDENCE ON TWO AFTERBODIES WITH A REARWARD FACING JET

by

A. H. CRAVEN

(Prepared under Ministry of Supply Contract 7/GEN/1473/PR3)

NOTE NO. 92.
December, 1958.

THE COLLEGE OF AERONAUTICS

CRANFIELD

The effect of body incidence on the forces and moments on two afterbodies with a rearward facing jet in a subsonic uniform flow.

- by -

A. H. Craven, Ph.D., M.Sc., D.C.Ae.

Prepared under Ministry of Supply Contract 7/GEN/1473/PR3

SUMMARY

This paper contains the results of an experimental investigation into the effect of a jet issuing from two afterbodies (one a right cylinder and the second conical) at incidence to a uniform subsonic flow. The tests were performed at a Reynolds Number of 0.3×10^6 based on body diameter and maximum tunnelvelocity.

The presence of the jet issuing from an afterbody at incidence significantly increases the magnitude of the normal force, axial force and pitching moment arising from the external forces but not including the direct reaction of the jet. On the bluff cylindrical afterbody the effect of the jet is comparable in magnitude to the effect of incidence. However the effect of the jet on the conical afterbody is secondary to the effect of incidence.

CONTENTS

LIST OF SYMBOLS

C_A	axial force coefficient in terms of total base area
C_J	jet thrust coefficient $\left(= \frac{mV_b}{\frac{1}{2}\rho U_o^2 S}\right)$
C_M	total pitching moment coefficient in terms of total base area
C_{M_B}	pitching moment coefficient on bluff afterbody due to base pressures
C_{M_N}	pitching moment coefficient on bluff afterbody due to side pressures
C_N	normal force coefficient in terms of total base area
C_p	pressure coefficient $\left(= \frac{p - p_o}{\frac{1}{2}\rho U_o^2}\right)$
d	body diameter
m	jet mass flow
p	static pressure (suffix o denotes free stream value)
r	radial distance from jet centre
R	radius of body
S	base area ($= \Pi R^2$)
U_o	free stream speed
V_b	equivalent jet velocity i.e. the velocity attained in an isentropic expansion from jet stagnation pressure to free stream static pressure
x	distance from jet exit along afterbody axis positive in upstream sense
α	afterbody incidence in degrees
θ	meridian angle
ρ	free stream density

1. Introduction

A previous paper (1) has given the results of experiments to determine the effect of an undeflected axi-symmetric jet upon the pressure distributions around representative afterbodies in a uniform subsonic stream and the effect of afterbody shape on the drag of the body at zero incidence. The effect of jet deflection on the flow round a blunt afterbody at zero incidence was the subject of a second paper (2) by the same author.

It is of interest to examine the effect of body incidence upon the forces on and the flow round an afterbody from which a jet is issuing and in particular to investigate the conditions which exist in the vicinity of the base. The afterbody at incidence without jet will experience a normal and an axial force by virtue of its incidence. The presence of a jet seriously complicates an analytic approach to the problem. Theoretical papers by Spence (3), Stratford (4) and Craven (5), and experimental investigations by Dimmock (6), Davidson (7) and others have explored the analogous two-dimensional problem. Reference (5) includes some consideration of the axi-symmetric problem but a solution has not yet been achieved. However an approximate application of slender body theory leads to the conclusion that, in inviscid flow, the interference between the jet and the flow around the afterbody is zero.

It is the purpose of the present paper to ascertain how the viscous effects, including the areas of separation, modify the result of slender body theory. Experiments were conducted to investigate the effects induced by the presence of the jet and in particular to determine the pressure distributions on the surface of a conical afterbody and on the base and side surfaces of a bluff cylindrical afterbody at incidence from which a jet issues. From the pressures, the side force, base drag and pitching moment induced on the afterbody by the interference of the jet with the subsonic free stream are calculated.

The experiments described herein are the third phase of a fuller investigation into the effect of jet flow sponsored by the Ministry of Supply under Contract No. 7/GEN1473/PR3. The author would like to thank Mr. F.M.Burrows for the preparation of Fig. 16, Mr. S. H. Lilley for the design and erection of the equipment, Mr. H. Stanton for the care and enthusiasm with which he made the models and the aerodynamic laboratory assistants who were responsible for taking the experimental measurements.

2. Apparatus

2.1. The wind tunnel and instrumentation

The tests were performed in a straight-through wind tunnel having a closed working section measuring 3 ft. square. The compressed air supply for the jet was led to the working section in a $3\frac{1}{2}$ in. diameter pipe along the centre line of the tunnel. The supply pipe was threaded at its downstream end to take the angled elbows necessary to give the afterbodies the required angle of incidence. The supply pipe was encased in a duralumin sleeve 4 in. in diameter, the space between the sleeve and the supply pipe being occupied by the pressure tubes.

The surface pressures on the models were read from a multitube water manometer.

2.2. The models

Two models were used in these tests :-

(i) a right cylinder 4" diameter and 12" long
(ii) a conical cylinder tapering from 4" to $\frac{3}{4}$" diameter in a length of 9" giving a boat-tail angle of $10\frac{1}{4}^{\circ}$.

The models were turned from light alloy. The internal cavity of each model was machined to give a smooth internal flow into a parallel sided jet $\frac{3}{4}$" in diameter issuing from the model along its centre line. An internal gauze screen was fitted between the model and the angled elbow to eliminate non-uniformities in the compressed air flow from the supply pipe into the model's pressure cavity.

Polythene tubing for pressure measurements was let into slots along the model's generators at angular intervals of $22\frac{1}{2}^{\circ}$ and secured with araldite.

3. Scope of the tests

The tests on each of the models covered a range of free stream speeds from 50 to 100 f.p.s. and a range of "equivalent" jet speeds from 0 to 1500 f.p.s. The equivalent jet speed is that calculated from the jet blowing pressure assuming isentropic expansion to free stream pressure. Defining the thrust coefficient C_J by

$$C_J = \frac{m V_b}{\frac{1}{2}\rho U_o^2 S}$$

where m = jet mass flow (slugs/sec)

V_b = equivalent jet speed (ft/sec)

U_o = tunnel speed (ft/sec)

S = base area of model (sq.ft)

the range of jet thrust coefficient covered by these tests was $0 \leqslant C_J \leqslant 40$.

The models were set at a series of incidences in the range $0^\circ \leq \alpha \leq 15^\circ$. Within this range of incidence, it is felt that interference between the jet and the tunnel walls does not affect the results significantly.

4. Test procedure

The ordinary pressure plotting techniques were used in these tests. The details are given in ref.1.

5. Results

5.1. Presentation of results

As in the previous work the pressure coefficients and forces and moments were found to be presentable in terms of the non-dimensional thrust coefficient C_J. The jet and free stream velocities are, thereby, not used explicitly. This use of C_J is justified for two reasons; firstly it can be shown that the forces on the bodies are proportional to C_J^n (e.g. Fig. 17) and for given C_J the results are independent of tunnel speed; i.e, the effect of Reynolds Number based on free stream velocity is small.

The pressure distributions on the bluff cylindrical afterbody are given in the form of isobar patterns as follows :-

Fig. 2 (a) Base pressure distribution at zero incidence ($\alpha = 0^\circ$) for $C_J = 0, 1, 2, 4, 10, 20, 40$.

(b) Base pressure distribution $\alpha = 2^\circ, 5^\circ, 10^\circ, 15^\circ$ $C_J = 0$

(c) Base pressure distribution $\alpha = 2^\circ, 5^\circ, 10^\circ, 15^\circ$ $C_J = 1$

(d) Base pressure distribution $\alpha = 2^\circ, 5^\circ, 10^\circ, 15^\circ$ $C_J = 2$

(e) Base pressure distribution $\alpha = 2^\circ, 5^\circ, 10^\circ, 15^\circ$ $C_J = 4$

(f) Base pressure distribution $\alpha = 2^\circ, 5^\circ, 10^\circ, 15^\circ$ $C_J = 10$

(g) Base pressure distribution $\alpha = 2^\circ, 5^\circ, 10^\circ, 15^\circ$ $C_J = 20$

(h) Base pressure distribution $\alpha = 2^\circ, 5^\circ, 10^\circ, 15^\circ$ $C_J = 40$

Fig. 5 (a) Side pressure distribution (not in isobar form) for zero incidence plotted against $\frac{x}{d}$ for C_J = 0, 1, 2, 4, 10, 20, 40.

(b) Side pressure distribution $\alpha = 2^\circ, 5^\circ, 10^\circ, 15^\circ$ $C_J = 0$

(c) Side pressure distribution $\alpha = 2^\circ, 5^\circ, 10^\circ, 15^\circ$ $C_J = 1$

(d) Side pressure distribution $\alpha = 2^\circ, 5^\circ, 10^\circ, 15^\circ$ $C_J = 2$

(e) Side pressure distribution $\alpha = 2^\circ, 5^\circ, 10^\circ, 15^\circ$ $C_J = 4$

(f) Side pressure distribution $\alpha = 2^\circ, 5^\circ, 10^\circ, 15^\circ$ $C_J = 10$

(g) Side pressure distribution $\alpha = 2^\circ, 5^\circ, 10^\circ, 15^\circ$ $C_J = 20$

(h) Side pressure distribution $\alpha = 2^\circ, 5^\circ, 10^\circ, 15^\circ$ $C_J = 40$

The origin for the meridian angle θ is shown in Fig. 1. The base and side distributionsare thus symmetrical about a vertical plane through the body centre-line. Hence the isobar patterns for incidences of 2° and 5° and 10° and 15° are placed side by side for ready comparison. In Fig. 5 the isobars are plotted on axes of the meridian angle θ and of the non-dimensional distance $(\frac{x}{d})$ upstream of the base.

Typical radial pressure distributions on the base are given in Figs. 3 and 4. Fig. 3 shows the dependence of the pressure coefficient upon body incidence α and Fig. 4 gives the variation with meridian angle θ; both figures being plotted for fixed values of C_J.

By integrating the appropriate pressure distributions the coefficients of axial force, normal force, pitching moment due to base pressure variations, pitching moment due to side pressure variations and total pitching moment about the centre of the base have been calculated and are given in Figs. 6 - 10 respectively plotted against C_J for given values of incidence and against incidence for particular values of C_J.

The pressure distributions on the tapered afterbody are given as isobar patterns as follows :-

Fig. 11 (a) Side pressure distribution (not in isobar form) for zero incidence plotted against $\frac{x}{d}$ for C_J = 0, 1, 2, 4, 10, 20, 40.

(b) Side pressure distribution $\alpha = 2^\circ, 5^\circ, 10^\circ, 15^\circ$ $C_J = 0$

(c) Side pressure distribution $\alpha = 2^\circ, 5^\circ, 10^\circ, 15^\circ$ $C_J = 1$

(d) Side pressure distribution $\alpha = 2^\circ, 5^\circ, 10^\circ, 15^\circ$ $C_J = 2$

(e) Side pressure distribution $\alpha = 2^\circ, 5^\circ, 10^\circ, 15^\circ$ $C_J = 4$

(f) Side pressure distribution $\alpha = 2^\circ, 5^\circ, 10^\circ, 15^\circ$ $C_J = 10$

(g) Side pressure distribution $\alpha = 2^\circ, 5^\circ, 10^\circ, 15^\circ$ $C_J = 20$

(h) Side pressure distribution $\alpha = 2^\circ, 5^\circ, 10^\circ, 15^\circ$ $C_J = 40$

Again the pressure distribution on the tapered body is symmetrical about the vertical plane through the body centre line. By integration of the pressure coefficients, the coefficients of axial force, normal force and pitching moment about the centre of the jet were calculated and are given in Figs. 12 - 14 respectively plotted as for the bluff cylindrical afterbody.

In all the curves drawn the jet has not reached the overchoked condition.

5.2. The pressure distribution on the bluff afterbody

5.2.1. The base pressures (Fig. 2a - h)

The general trend of the pressure distribution on the base remains unaltered as body incidence is increased. The base suction increases with radial distance to a peak at $\frac{r}{R} = .7$ approximately and then decreases (Figs. 3 and 4). For any particular value of C_J and $\frac{r}{R}$ (except very close to the jet exit), the variation of pressure coefficient with meridian angle shows a steady increase in suction from $\theta = 0^\circ$ to 135° and thereafter remains sensibly constant (Fig. 4). In other words the maximum suction occurs over a narrow band situated at $\frac{r}{R} = .7$ approximately and stretching for about 45° on either side of the plane of symmetry. The radial position of the peak suction moves outwards as the incidence increases, e.g. peak suction occurs at $\frac{r}{R} = .70$ for $\alpha = 0^\circ$

at $\frac{r}{R} = .71$ for $\alpha = 5^\circ$

at $\frac{r}{R} = .73$ for $\alpha = 10^\circ$

and at $\frac{r}{R} = .78$ for $\alpha = 15^\circ$

in the case $\theta = 180^\circ$, $C_J = 40$ (Fig. 3).

Furthermore the radial position of the peak section moves outwards as meridian angle θ changes from 0° to 90° and then slightly inwards again to $\theta = 180^\circ$, e.g. in the case when $\alpha = 10^\circ$, $C_J = 20$ (Fig. 4)

peak motion occurs at $\frac{r}{R} = .64$ for $\theta = 0^\circ$

at $\frac{r}{R} = .70$ for $\theta = 45^\circ$

at $\frac{r}{R} = .75$ for $\theta = 90^\circ$

at $\frac{r}{R} = .72$ for $\theta = 135^\circ$

and at $\frac{r}{R} = .73$ for $\theta = 180^\circ$

At zero body incidence and at $\frac{r}{R} = 0.6$ approximately for all values of C_J there appeared a suction peak followed at a slightly larger radius by a second and larger suction peak. The same effect is noted with the afterbody at incidence but in a modified form. At $\theta < 45^\circ$ the effect is absent. As θ increases the effect becomes apparent but the fall and subsequent rise covers a much larger region than for zero incidence. The magnitude of the angle of incidence does not seem to affect this phenomenon.

The jet choked at a particular value of C_J for a given freestream speed. A small increase of C_J above this value caused a rapid decrease in suction over the base by about ten per cent of its value when the jet choked. The values of the pressure coefficient remained constant if C_J was further increased. The effect was the same for all body incidences. This feature has been omitted from the isobar patterns to avoid confusion.

5.2.2. <u>The side pressure distributions</u> (Figs. 5a - h)

As on the base, the presence of the jet increases the slight suction on the side of the body. As in the previous experiments it was found that the jet had negligible effect at distances greater than two body diameters upstream of the base. For any value of C_J and any value of $\frac{x}{d}$ the suction rises with increase of meridian angle θ. At small incidences this trend is maintained over the whole range of θ. At incidences greater than 5° however a suction peak occurs between $\theta = 67^\circ$ and 90° and further increase of θ results in a reduction of suction until at $\theta = 180^\circ$ (the upper surface) the pressure is not appreciably different from that on the under surface ($\theta = 0^\circ$) for the same values of $C_J = \frac{x}{d}$.

Except at points close to the base ($\frac{x}{d} < .05$) the side pressure distributions for choked and overchoked jet coincided for the same tunnel speed and incidence.

5.3. The Forces and Moments on the bluff afterbody

The force and moment coefficients were obtained by dividing the particular force by $\frac{1}{2}\rho U_o^2 S$, S being the maximum cross-sectional area of the afterbody, and the moment by $\frac{1}{2}\rho U_o^2 Sd$ where d is the maximum afterbody diameter. The origin for moments is the centre of the jet orifice.

5.3.1. Base drag (Fig. 6)

The base drag is presented as the axial force in the direction of the afterbody's centre line. The base drag coefficient increases with increase of C_J for all values of body incidence. The increase is large initially but moderates as C_J increases.

A second important feature is that for any value of C_J other than zero within the range of these experiments, the drag decreased as the incidence increased up to $2^\circ - 5^\circ$, depending upon the C_J involved, thereafter increasing with incidence.

The effect of overchoking the jet is the same as reported previously (ref. 1).

5.3.2. Normal force (Fig. 7)

The normal force, jet off, measured positively in the direction $\theta = 180^\circ$ and perpendicular to the body centre line shows a considerable rise as the incidence is increased. Furthermore the effect of the jet is to produce a normal force augmenting that due to incidence alone. It is evident that, except for the large incidences, the normal force depends only slightly upon the effect of the jet. Indeed it is only at $\alpha = 15^\circ$ that an appreciable increase in C_N occurs at values of C_J greater than 10.

5.3.3. The pitching moment

All pitching moments are measured about the centre of the base and taken positive in the nose-up sense.

5.3.3.1. Moment due to base pressures (Fig. 8)

The pitching moment due to the variation of the base pressure distribution with incidence and C_J is found to be positive for all values of C_J and α within the range of the experiments. Increase of C_J and α cause a rise in pitching moment except at high incidence and low C_J where there is a tendency for the value of C_{M_B} to fall for further increase of C_J.

5.3.3.2. Moment due to the side pressures (Fig. 9)

The moment due to the side pressures is nose-up for all values of incidence and C_J. The magnitude of C_{M_N} increases sharply with increase of incidence up to 2° for all values of C_J. For $C_J \leq 20$ there is a further slight increase up to $\alpha = 10^\circ$ and then a small decrease as α approaches 15°. For $C_J > 20$ the value of C_{M_N} decreases with increase of incidence until at $\alpha = 15^\circ$ it differs only slightly from the values for $C_J = 20$.

These results are to be expected from the side pressure distributions (Fig. 5a - g). For $\alpha = 5^\circ$ for the higher values of C_J, and $\alpha = 10^\circ$ and 15° for all C_J the pressure distributions show the peak suctions occurring in the region $\theta = 90^\circ$ where they have little effect on moment. The pressures on the upper and lower surfaces are nearly the same and hence an almost constant value of C_{M_N} is to be expected at the high incidences.

5.3.3.3. Total pitching moment (Fig. 10)

The sum of the base and side moments is the total pitching moment acting on the afterbody. It increases, in general, with incidence and C_J. However, for small values of C_J, the increase of C_M with α is very small for values of incidence greater than 5°.

5.4. The pressure distribution on the tapered afterbody (Fig. 11a - h)

The pressure distributions on the tapered afterbody which were symmetric about the body centre line at zero incidence now showed marked variations with change in meridian angle, although the variation along generators showed the same general trends as at $\alpha = 0^\circ$. It was noted that, at the higher incidences, suction peaks developed at $\theta = 45^\circ$ approximately.

Because of the possible errors due to the proximity to the elbow, the pressure distributions on the parallel portion of the afterbody ($x/d > 2.5$) are not given.

5.5. The forces and moments on the tapered afterbody

The forces and pitching moments are in the directions and senses defined in paragraph 5.3.3.

5.5.1. The axial force (Fig. 12)

Increase of incidence causes a large increase in the axial force coefficient and increase of C_J further increases C_A. The effect of the jet is only very slight for $C_J < 10$ at all incidences and for all C_J at zero incidence. For $C_J > 10$ the jet interference significantly augments the drag due to incidence.

5.5.2. The normal force (Fig. 13)

As with the axial force, incidence is the major factor affecting the normal force, the jet interference having only a secondary effect. Values of C_J less than 10 seem to have no effect at all and for $C_J = 40$ the increment in normal force coefficient due to the jet interference is only 30% of that due to incidence. It should be noted that as with ordinary conical afterbodies the normal force is negative.

5.5.3. The pitching moment (Fig. 14)

The pitching moment is negative for all values of C_J and incidence. Up to $\alpha = 5^\circ$ increase of incidence causes an increase in the magnitude of the pitching moment coefficient. Further increase of incidence is accompanied by a slight reduction in the magnitude of C_M. The presence of the jet has a negligible effect on the pitching moment.

6. Discussion

6.1. Accuracy of results

The jet supply pressure during any one test was maintained at the required value within limits of 2%. The tunnel speed could be kept accurate to within 1% and the surface pressures were measured to 0.02 in. of water. The overall error in the pressure coefficients and the force and moment coefficients is therefore expected to be less than 5%.

6.2. The flow around the cylindrical afterbody

It is found that setting the afterbody at incidence causes major modification of the toroidal vortex system which is set up when the jet issues from the centre of the bluff base of the undeflected afterbody (ref.1). Except in the vertical plane of symmetry the flow on the base is no longer radial but curves from an attachment line at $\frac{r}{R} = .3$ approximately to a

separation line at $\frac{r}{R} = .8$ approximately. This is shown in Fig. 15 which is drawn from a series of surface flow pictures. There is also a weak flow into the separation line inwards from the edge of the base ($\frac{r}{R} = 1$) and the air entrained into the jet at its exit curls into the jet from the attachment line. The separation and attachment lines show little evidence of eccentricity for small incidences but at the higher incidences a degree of eccentricity in the separation line is apparently equivalent to $\frac{r}{R} = .1$. This is consistent with the form and extent of the radial pressure distribution. The presence of the separation line is to be expected in view of the adverse pressure gradient outboard of the peak suction at $\frac{r}{R} = .8$ approximately and the attachment line is confirmed by the minimum suction that occurs at $\frac{r}{R} = .3$ approximately. This and the degree of eccentricity can be seen more clearly if the pressure coefficients are plotted against radial distance for a series of meridian angles at one incidence and at one meridian angle for a series of incidences (e.g. Figs. 3 and 4).

In the lower plane of symmetry ($\theta = 0^\circ$) there is relatively little variation in pressure coefficient with radius. The surface flow patterns near $\theta = 0^\circ$ show little accretion of fluid and the attachment line is very indefinite. As the meridian angle increases so the radial variation of the base suction coefficient is increased until in the region $135^\circ < \theta < 180^\circ$ the pressure variation is greatest. The separation is strongest in this same region as indicated by the high suction lobes in that region on the isobar patterns. The boundary layer which separates from the base appears to roll up and form a pair of spiral vortex sheets. These vortices originate near the base in the lower plane of symmetry and increase in strength as they move round the base until they separate in the region $135^\circ < \theta < 180^\circ$. They pass downstream and eventually must merge into the jet (Fig. 16).

There are no features in the surface flow patterns which correspond to the first suction peak at $\frac{r}{R} = 0.6$ (Figs. 4 and 15). The form of the pressure distribution is, however, consistent with the development of a laminar type boundary layer up to $\frac{r}{R} = 0.6$ followed by a laminar separation and turbulent reattachment. Turbulent separation then occurs, as stated above, at $\frac{r}{R} = 0.8$.

The pressure distributions on the side of the bluff afterbody suggest that the flow over the afterbody with jet is not significantly different from that at the same incidence with no jet. At 2° incidence it would appear that the cross flow does not separate for any value of C_J. At 5° incidence separation occurs at $\theta = 135^\circ$ except for $C_J = 40$ and in this case the effect of entrainment into the jet is sufficient to prevent separation on the side surfaces. At the higher incidences separation occurs as one would expect at $\theta = 70^\circ$ approximately, the separated boundary layers rolling up to form the characteristic vortex pair.

The mixing region beyond about two body diameters downstream of the base contains three intially distinct flows; the jet, the pair of vortex sheets shed from the base and the pair shed from the sides of the afterbody (Fig. 16). Yawmeter investigations in the wake did not give sufficient detail to determine the exact nature of the mixing processes between the vortices and the jet. From tuft investigations it was found that the inner separated regions close to the base of the body extended to about one body diameter downstream of the base.

6.3. The flow pattern around the conical afterbody

At low values of C_J ($C_J < 2$) the flow around the conical afterbody is little affected by the jet. The flow appears to separate at about one body diameter upstream of the jet exit and only for $C_J > 2$ is the entrainment into the jet sufficient to cause reattachment. At the larger incidences the pressure distributions show evidence of boundary layer separation at $\theta = 45^\circ$ with the separated boundary layers rolling up to form the pair of rolled-up vortex sheets characteristic of a body of revolution at incidence. At the higher values of C_J the entrainment effect of the jet is to reduce the strength of the vortices since less flow is fed into them. This has the effect of reducing the suction peaks on the sides of the body.

6.4. Dependence of the results on C_J^n

If the results for the normal force acting on the bluff afterbody are expressed in the form $\log(C_N - C_{N_{C_J = 0}})$ and plotted against $\log C_J$ (Fig. 17) it is found that, for each incidence, a straight line is obtained the slope increasing with incidence indicating that the incidence effect and jet effect are additive and that

$$C_N - C_{N_{C_J = 0}} \sim C_J^n \; g_1(\alpha)$$

where n is a constant depending upon the incidence α, and $g_1(\alpha)$ is zero when $\alpha = 0^\circ$.

It is noticed that, for incidences considered, $n/\sin^{\frac{1}{2}}\alpha$ is a constant and equal to 1.55 approximately.

α	2°	5°	10°	15°
n	0.290	0.455	0.640	0.792
$\sqrt{\sin \alpha}$	0.1868	0.2953	0.4166	0.5058
$n/\sqrt{\sin \alpha}$	1.55	1.54	1.54	1.56

When $\log(C_A - C_{A_{C_J = 0}})$ is similarly plotted (Fig. 18) it is again seen that $C_A - C_{A_{C_J = 0}}$ is proportional to $C_J^n \, g_2(\alpha)$. The value of n is 0.58 approximately and appears to be independent of incidence.

While the normal force coefficient for the conical afterbody does obey a law of the form

$$C_N - C_{N_{C_J = 0}} \sim C_J^n \, g_3(\alpha)$$

the relation between n and α cannot be stated as precisely as for the bluff afterbody. To within 20% accuracy the relation $\frac{n}{\sin^{\frac{1}{2}}\alpha} = 4.7$ covers the experimental points. The axial force on the conical afterbody is predominantly dependent upon incidence; the experimental evidence is not sufficient to deduce a functional relationship between axial force and jet momentum coefficient.

7. Conclusions

(i) The presence of a jet issuing from the afterbody at incidence significantly increases the magnitude of the normal force, drag and pitching moment on a bluff cylindrical afterbody and a conical afterbody. This effect is in addition to the normal jet reaction.

(ii) On the bluff cylindrical afterbody the effect of the jet is comparable in magnitude to the effect of incidence. The effect of the jet on the conical afterbody is secondary to the effect of incidence.

(iii) Typical magnitudes of these effects on the cylindrical afterbody are as follows :-

At 15° incidence the normal force coefficient was raised from 0.27 at $C_J = 0$ to 0.73 at $C_J = 40$. The base drag coefficient was raised from 0.31 to 1.38 for the same increase in C_J but the increment in drag coefficient is roughly independent of incidence.

(iv) On the conical afterbody the maximum effect was experienced at 15° incidence where the axial force coefficient was raised from 0.81 to 0.97 by increasing C_J from 0 to 40. The corresponding values for $\alpha = 0^{\circ}$ are 0.11 and 0.13. The normal force coefficient at 15° incidence changed from -0.46 to -0.59 for the same range of C_J.

(v) The pitching moment on the bluff afterbody was predominantly due to the pressure variations on the base whereas on the conical afterbody it was sensibly independent of jet interference.

8. References

1. Craven, A.H. — The interference of a rearward facing jet on the flow over three representative afterbody shapes in a uniform subsonic flow. College of Aeronautics Note No.60, April,1957.

2. Craven, A.H. — The effect of jet deflection on the interference of a rearward facing jet with the flow over an afterbody in a uniform subsonic flow. College of Aeronautics Note No.70, October,1957.

3. Spence, D.A. — Treatment of the jet flap by thin aerofoil theory. R.A.E. Report Aero.2568. November, 1955.

4. Stratford, B.S. — Mixing and the jet flap. Aero. Quarterly, Vol.7, August, 1956.

5. Craven, A.H. — A potential flow model for the flow about a nacelle with jet. College of Aeronautics Report No.101, March, 1956.

6. Dimmock, N.A. — An experimental introduction to the jet flap. N.G.T.E. Report R.175, and Some further jet flap experiments. N.G.T.E. Memorandum M.255.

7. Davidson, I. — The jet flap. Journal of the Royal Aeronautical Society, January, 1956.

TABLE 1 BASE SUCTION COEFFICIENTS 2° INCIDENCE

$\frac{r}{R}$	0.237	0.287	0.337	0.387	0.437	0.487	0.537	0.587	0.637	0.687	0.737	0.787	0.837	0.887	0.937
C_J															
$\theta = 0^\circ$															
0	0.162	0.154	0.137	0.137	0.137	0.120	0.120	0.130	0.123	0.127	0.135	0.135	0.148	0.162	0.170
1	0.203	0.203	0.203	0.200	0.194	0.190	0.186	0.178	0.178	0.172	0.172	0.172	0.188	0.198	0.212
2	0.318	0.297	0.246	0.218	0.194	0.190	0.182	0.178	0.180	0.186	0.188	0.183	0.178	0.178	0.183
4	0.314	0.297	0.287	0.289	0.294	0.298	0.306	0.309	0.338	0.358	0.358	0.343	0.326	0.292	0.257
6	0.314	0.306	0.287	0.295	0.317	0.326	0.342	0.361	0.394	0.416	0.407	0.404	0.398	0.361	0.318
8	0.318	0.306	0.294	0.307	0.329	0.350	0.378	0.413	0.456	0.493	0.503	0.514	0.474	0.443	0.394
10	0.320	0.306	0.300	0.315	0.346	0.378	0.414	0.488	0.549	0.581	0.623	0.648	0.602	0.542	0.482
15	0.375	0.344	0.332	0.354	0.407	0.462	0.539	0.624	0.674	0.667	0.720	0.703	0.651	0.570	0.514
20	0.400	0.384	0.376	0.391	0.471	0.574	0.684	0.790	0.826	0.774	0.834	0.794	0.710	0.618	0.553
25	0.414	0.396	0.398	0.436	0.528	0.641	0.751	0.861	0.903	0.856	0.894	0.867	0.767	0.667	0.602
30	0.421	0.408	0.426	0.494	0.597	0.727	0.836	0.943	0.986	0.954	0.966	0.942	0.826	0.726	0.664
35	0.421	0.426	0.453	0.547	0.649	0.817	0.928	1.018	1.078	1.032	1.029	0.984	0.882	0.788	0.739
40	0.424	0.446	0.500	0.612	0.726	0.903	1.042	1.106	1.183	1.121	1.074	1.026	0.941	0.866	0.814
$\theta = 22\frac{1}{2}^\circ$															
0	0.160	0.158	0.144	0.144	0.140	0.137	0.137	0.135	0.135	0.130	0.130	0.140	0.156	0.165	0.172
1	0.206	0.200	0.208	0.204	0.212	0.200	0.194	0.196	0.212	0.218	0.216	0.212	0.196	0.194	0.194
2	0.308	0.297	0.261	0.228	0.220	0.224	0.228	0.232	0.267	0.256	0.244	0.240	0.226	0.212	0.205
4	0.320	0.310	0.284	0.308	0.326	0.342	0.356	0.376	0.408	0.414	0.418	0.406	0.381	0.338	0.288
6	0.314	0.311	0.305	0.322	0.353	0.389	0.408	0.438	0.465	0.486	0.472	0.458	0.432	0.382	0.336
8	0.318	0.306	0.318	0.337	0.386	0.438	0.458	0.484	0.522	0.547	0.551	0.554	0.514	0.469	0.404
10	0.326	0.320	0.320	0.356	0.412	0.497	0.526	0.572	0.611	0.630	0.647	0.647	0.602	0.540	0.476
15	0.370	0.344	0.354	0.389	0.443	0.534	0.612	0.681	0.719	0.718	0.741	0.728	0.693	0.627	0.553
20	0.386	0.358	0.371	0.403	0.476	0.598	0.708	0.784	0.864	0.854	0.869	0.837	0.772	0.678	0.612
25	0.408	0.392	0.414	0.451	0.549	0.660	0.790	0.891	0.951	0.946	0.964	0.915	0.839	0.742	0.665
30	0.421	0.421	0.457	0.516	0.622	0.743	0.886	0.976	1.038	1.012	1.026	0.996	0.884	0.789	0.719
35	0.421	0.442	0.492	0.570	0.678	0.842	0.953	1.061	1.122	1.114	1.102	1.042	0.951	0.846	0.786
40	0.421	0.461	0.521	0.661	0.770	0.934	1.058	1.158	1.228	1.206	1.178	1.104	1.002	0.915	0.867
$\theta = 45^\circ$															
0	0.162	0.158	0.140	0.140	0.137	0.137	0.137	0.132	0.132	0.132	0.135	0.142	0.154	0.167	0.178
1	0.216	0.203	0.203	0.200	0.216	0.200	0.207	0.218	0.234	0.254	0.240	0.218	0.200	0.188	0.184
2	0.306	0.284	0.250	0.237	0.254	0.268	0.276	0.298	0.324	0.306	0.348	0.306	0.273	0.254	0.242
4	0.316	0.306	0.309	0.326	0.368	0.400	0.421	0.458	0.385	0.476	0.490	0.464	0.421	0.361	0.312
6	0.306	0.300	0.317	0.350	0.406	0.461	0.484	0.512	0.543	0.542	0.547	0.507	0.486	0.412	0.360
8	0.318	0.312	0.330	0.373	0.452	0.535	0.556	0.580	0.607	0.613	0.627	0.588	0.551	0.467	0.412
10	0.363	0.343	0.348	0.403	0.500	0.610	0.635	0.662	0.675	0.691	0.691	0.662	0.623	0.538	0.482
15	0.366	0.343	0.375	0.418	0.484	0.589	0.702	0.759	0.791	0.780	0.796	0.761	0.716	0.630	0.565
20	0.380	0.343	0.402	0.426	0.498	0.610	0.762	0.851	0.920	0.886	0.934	0.878	0.814	0.742	0.676
25	0.403	0.403	0.434	0.481	0.572	0.691	0.836	0.932	1.004	0.969	1.023	0.954	0.876	0.786	0.713
30	0.426	0.463	0.471	0.548	0.654	0.782	0.910	1.016	1.100	1.064	1.106	1.032	0.944	0.848	0.772
35	0.424	0.498	0.548	0.612	0.731	0.876	0.989	1.104	1.186	1.170	1.194	1.104	1.018	0.909	0.827
40	0.412	0.491	0.552	0.697	0.820	0.974	1.086	1.200	1.287	1.263	1.302	1.206	1.094	0.982	0.896

TABLE 1 (Continued)

C_J	$\frac{r}{R}$ 0.237	0.287	0.337	0.387	0.437	0.487	0.537	0.587	0.637	0.687	0.737	0.787	0.837	0.887	0.937
$\theta = 67\frac{1}{2}^\circ$															
0	0.162	0.160	0.152	0.146	0.142	0.142	0.137	0.139	0.135	0.140	0.142	0.146	0.154	0.167	0.178
1	0.241	0.228	0.238	0.274	0.288	0.288	0.279	0.279	0.276	0.289	0.294	0.279	0.266	0.252	0.241
2	0.289	0.270	0.271	0.287	0.310	0.329	0.341	0.352	0.352	0.342	0.336	0.322	0.298	0.286	0.263
4	0.321	0.314	0.342	0.385	0.416	0.456	0.472	0.485	0.504	0.492	0.504	0.481	0.465	0.415	0.371
6	0.326	0.328	0.351	0.406	0.450	0.511	0.528	0.544	0.560	0.564	0.562	0.556	0.519	0.468	0.437
8	0.335	0.352	0.385	0.429	0.496	0.558	0.584	0.618	0.632	0.648	0.657	0.645	0.602	0.537	0.491
10	0.382	0.396	0.402	0.458	0.532	0.612	0.664	0.709	0.719	0.733	0.736	0.733	0.694	0.622	0.566
15	0.398	0.378	0.436	0.493	0.556	0.638	0.728	0.796	0.809	0.821	0.830	0.818	0.772	0.714	0.643
20	0.416	0.375	0.496	0.542	0.613	0.696	0.809	0.886	0.952	0.934	0.956	0.918	0.862	0.806	0.736
25	0.431	0.415	0.509	0.586	0.654	0.751	0.878	0.957	1.028	1.004	1.038	0.986	0.916	0.846	0.778
30	0.448	0.463	0.546	0.621	0.718	0.830	0.952	1.034	1.122	1.109	1.128	1.071	0.981	0.898	0.817
35	0.429	0.478	0.579	0.655	0.762	0.896	1.009	1.116	1.208	1.188	1.206	1.126	1.036	0.957	0.854
40	0.410	0.490	0.581	0.702	0.828	0.978	1.086	1.206	1.324	1.291	1.311	1.219	1.108	1.013	0.902
$\theta = 90^\circ$															
0	0.162	0.156	0.146	0.142	0.140	0.137	0.137	0.137	0.137	0.140	0.140	0.149	0.158	0.167	0.174
1	0.279	0.265	0.284	0.320	0.331	0.336	0.341	0.341	0.342	0.339	0.346	0.329	0.316	0.305	0.294
2	0.285	0.260	0.287	0.320	0.359	0.394	0.426	0.418	0.390	0.363	0.346	0.332	0.318	0.309	0.287
4	0.328	0.357	0.409	0.441	0.482	0.509	0.512	0.517	0.522	0.517	0.529	0.504	0.487	0.452	0.424
6	0.336	0.376	0.420	0.459	0.506	0.542	0.567	0.588	0.597	0.597	0.607	0.589	0.549	0.514	0.489
8	0.371	0.395	0.441	0.481	0.540	0.586	0.622	0.661	0.669	0.692	0.691	0.684	0.636	0.598	0.554
10	0.427	0.440	0.468	0.506	0.571	0.632	0.691	0.742	0.764	0.776	0.784	0.786	0.747	0.695	0.632
15	0.435	0.429	0.515	0.584	0.644	0.707	0.775	0.838	0.862	0.860	0.871	0.862	0.815	0.770	0.704
20	0.448	0.421	0.600	0.674	0.731	0.798	0.872	0.934	0.976	0.954	0.986	0.948	0.900	0.852	0.798
25	0.467	0.437	0.603	0.690	0.754	0.834	0.925	0.990	1.060	1.033	1.069	1.002	0.945	0.888	0.823
30	0.473	0.458	0.612	0.702	0.786	0.883	0.996	1.054	1.154	1.109	1.160	1.065	1.002	0.930	0.847
35	0.439	0.472	0.612	0.711	0.804	0.929	1.048	1.129	1.261	1.237	1.241	1.129	1.048	0.972	0.872
40	0.400	0.486	0.600	0.716	0.842	0.986	1.100	1.218	1.387	1.379	1.296	1.206	1.114	1.026	0.906
$\theta = 112\frac{1}{2}^\circ$															
0	0.162	0.162	0.154	0.184	0.144	0.144	0.137	0.137	0.142	0.148	0.152	0.156	0.162	0.170	0.178
1	0.276	0.281	0.299	0.318	0.331	0.339	0.346	0.348	0.350	0.348	0.348	0.322	0.310	0.298	0.276
2	0.280	0.293	0.308	0.346	0.378	0.421	0.444	0.450	0.423	0.386	0.366	0.344	0.321	0.309	0.296
4	0.330	0.341	0.396	0.431	0.472	0.492	0.512	0.515	0.531	0.519	0.530	0.524	0.502	0.456	0.421
6	0.339	0.341	0.408	0.462	0.514	0.546	0.584	0.608	0.625	0.623	0.642	0.626	0.576	0.521	0.496
8	0.366	0.380	0.441	0.504	0.568	0.612	0.658	0.696	0.718	0.731	0.746	0.716	0.662	0.611	0.572
10	0.405	0.418	0.452	0.512	0.600	0.688	0.750	0.790	0.821	0.841	0.857	0.821	0.764	0.711	0.668
15	0.431	0.429	0.486	0.571	0.651	0.732	0.821	0.876	0.910	0.938	0.938	0.894	0.839	0.792	0.726
20	0.452	0.436	0.535	0.632	0.706	0.804	0.911	0.984	1.022	1.026	1.011	0.979	0.926	0.874	0.827
25	0.476	0.451	0.562	0.659	0.748	0.856	0.962	1.046	1.100	1.100	1.106	1.032	0.971	0.908	0.851
30	0.492	0.462	0.574	0.687	0.799	0.918	1.024	1.114	1.181	1.181	1.164	1.098	1.031	0.962	0.883
35	0.478	0.478	0.586	0.715	0.824	0.995	1.102	1.208	1.278	1.294	1.246	1.154	1.096	1.006	0.915
40	0.473	0.489	0.586	0.736	0.875	1.031	1.156	1.326	1.385	1.402	1.308	1.232	1.156	1.061	0.958

TABLE 1 (Continued)

$\frac{r}{R}$	0.237	0.287	0.337	0.387	0.437	0.487	0.537	0.587	0.637	0.687	0.737	0.787	0.837	0.887	0.937
C_J															
$\theta = 135^\circ$															
0	0.162	0.156	0.150	0.146	0.144	0.141	0.139	0.139	0.144	0.150	0.158	0.165	0.169	0.175	0.180
1	0.284	0.307	0.312	0.319	0.331	0.346	0.354	0.361	0.354	0.368	0.343	0.322	0.312	0.296	0.274
2	0.284	0.318	0.346	0.388	0.412	0.435	0.464	0.486	0.449	0.417	0.387	0.361	0.334	0.314	0.296
4	0.337	0.324	0.384	0.426	0.456	0.482	0.516	0.531	0.547	0.532	0.565	0.549	0.520	0.466	0.421
6	0.351	0.342	0.403	0.459	0.514	0.567	0.609	0.639	0.662	0.654	0.687	0.654	0.608	0.544	0.503
8	0.373	0.367	0.424	0.493	0.575	0.654	0.702	0.731	0.783	0.787	0.802	0.758	0.698	0.629	0.594
10	0.398	0.406	0.452	0.531	0.646	0.752	0.814	0.849	0.884	0.914	0.957	0.865	0.800	0.732	0.684
15	0.436	0.422	0.479	0.555	0.663	0.784	0.877	0.928	0.971	1.021	1.004	0.926	0.872	0.816	0.766
20	0.484	0.447	0.518	0.580	0.694	0.819	0.942	1.026	1.088	1.100	1.052	1.014	0.958	0.905	0.862
25	0.491	0.465	0.530	0.627	0.752	0.885	1.002	1.103	1.144	1.172	1.114	1.074	1.006	0.951	0.888
30	0.507	0.473	0.544	0.679	0.799	0.967	1.076	1.209	1.226	1.264	1.196	1.137	1.073	1.002	0.926
35	0.518	0.486	0.557	0.715	0.851	1.024	1.147	1.302	1.302	1.361	1.257	1.189	1.130	1.043	0.961
40	0.521	0.502	0.574	0.763	0.922	1.102	1.224	1.416	1.396	1.437	1.332	1.266	1.208	1.098	1.002
$\theta = 167\frac{1}{2}^\circ$															
0	0.162	0.156	0.150	0.150	0.144	0.144	0.141	0.141	0.144	0.144	0.155	0.158	0.169	0.172	0.172
1	0.286	0.307	0.310	0.312	0.331	0.348	0.354	0.361	0.360	0.374	0.348	0.326	0.328	0.314	0.310
2	0.286	0.316	0.336	0.372	0.406	0.428	0.460	0.474	0.449	0.426	0.412	0.366	0.350	0.317	0.312
4	0.328	0.311	0.348	0.381	0.421	0.461	0.492	0.516	0.532	0.532	0.528	0.532	0.501	0.458	0.422
6	0.344	0.331	0.371	0.414	0.482	0.534	0.586	0.622	0.646	0.667	0.667	0.636	0.582	0.536	0.498
8	0.368	0.352	0.398	0.461	0.538	0.621	0.694	0.743	0.771	0.794	0.810	0.749	0.687	0.632	0.590
10	0.388	0.391	0.438	0.525	0.621	0.726	0.810	0.842	0.886	0.902	0.946	0.870	0.824	0.758	0.684
15	0.428	0.406	0.470	0.541	0.652	0.768	0.875	0.922	0.986	1.008	1.008	0.951	0.898	0.841	0.756
20	0.468	0.442	0.512	0.592	0.708	0.826	0.928	1.046	1.074	1.096	1.104	1.046	1.008	0.932	0.877
25	0.476	0.456	0.527	0.608	0.741	0.880	1.002	1.112	1.134	1.194	1.186	1.112	1.042	0.973	0.902
30	0.481	0.458	0.544	0.651	0.782	0.943	1.068	1.228	1.238	1.270	1.294	1.174	1.105	1.030	0.946
35	0.478	0.472	0.557	0.696	0.826	1.018	1.156	1.316	1.336	1.368	1.294	1.236	1.158	1.074	0.996
40	0.466	0.491	0.570	0.732	0.881	1.096	1.232	1.400	1.403	1.442	1.386	1.292	1.232	1.128	1.048
$\theta = 180^\circ$															
0	0.162	0.156	0.150	0.146	0.144	0.144	0.139	0.141	0.141	0.148	0.155	0.160	0.165	0.167	0.169
1	0.292	0.284	0.302	0.324	0.338	0.354	0.349	0.361	0.357	0.357	0.348	0.337	0.332	0.322	0.314
2	0.284	0.306	0.326	0.359	0.388	0.417	0.446	0.452	0.452	0.431	0.403	0.382	0.350	0.331	0.302
4	0.296	0.284	0.297	0.297	0.327	0.399	0.442	0.487	0.516	0.524	0.524	0.516	0.486	0.452	0.407
6	0.325	0.308	0.329	0.359	0.406	0.487	0.556	0.613	0.630	0.657	0.662	0.617	0.570	0.536	0.492
8	0.351	0.331	0.364	0.414	0.473	0.571	0.683	0.717	0.745	0.802	0.813	0.732	0.684	0.650	0.586
10	0.376	0.364	0.402	0.494	0.561	0.684	0.800	0.831	0.878	0.923	0.931	0.876	0.832	0.764	0.684
15	0.400	0.389	0.451	0.529	0.624	0.752	0.875	0.946	0.984	1.016	1.024	0.948	0.917	0.856	0.762
20	0.446	0.432	0.506	0.574	0.698	0.831	0.916	1.032	1.096	1.122	1.100	1.054	1.026	0.961	0.873
25	0.441	0.437	0.520	0.596	0.729	0.880	0.994	1.129	1.166	1.208	1.221	1.119	1.076	1.002	0.915
30	0.427	0.439	0.538	0.622	0.765	0.946	1.085	1.226	1.257	1.296	1.302	1.193	1.129	1.048	0.967
35	0.402	0.452	0.550	0.650	0.794	0.998	1.173	1.308	1.339	1.392	1.346	1.248	1.172	1.096	1.021
40	0.382	0.473	0.576	0.681	0.828	1.064	1.270	1.400	1.428	1.471	1.398	1.306	1.238	1.152	1.070

TABLE 2 BASE SUCTION COEFFICIENTS 5° INCIDENCE

C_J \ $\frac{r}{R}$	0.237	0.287	0.337	0.387	0.437	0.487	0.537	0.587	0.637	0.687	0.737	0.787	0.837	0.887	0.937
$\theta = 0^\circ$															
0	0.162	0.154	0.154	0.142	0.137	0.140	0.137	0.137	0.137	0.140	0.142	0.146	0.151	0.155	0.160
1	0.306	0.289	0.273	0.259	0.246	0.243	0.248	0.246	0.246	0.246	0.241	0.256	0.259	0.252	0.256
2	0.439	0.413	0.400	0.372	0.358	0.363	0.375	0.380	0.392	0.400	0.437	0.442	0.386	0.311	0.265
4	0.426	0.402	0.396	0.374	0.369	0.349	0.347	0.376	0.391	0.398	0.392	0.380	0.375	0.341	0.338
6	0.432	0.418	0.413	0.410	0.418	0.402	0.425	0.434	0.448	0.436	0.428	0.406	0.388	0.359	0.350
8	0.436	0.429	0.438	0.451	0.456	0.458	0.476	0.487	0.496	0.477	0.456	0.428	0.392	0.372	0.352
10	0.448	0.435	0.452	0.476	0.485	0.491	0.500	0.522	0.528	0.496	0.472	0.438	0.409	0.378	0.365
15	0.454	0.448	0.473	0.498	0.530	0.552	0.576	0.608	0.626	0.634	0.654	0.629	0.573	0.494	0.452
20	0.467	0.451	0.488	0.513	0.552	0.596	0.621	0.673	0.713	0.748	0.800	0.809	0.712	0.587	0.504
25	0.492	0.523	0.574	0.628	0.693	0.734	0.783	0.839	0.868	0.884	0.917	0.923	0.784	0.675	0.599
30	0.521	0.562	0.651	0.731	0.805	0.854	0.896	0.968	0.983	1.014	1.006	0.916	0.846	0.742	0.677
35	0.559	0.590	0.725	0.829	0.931	0.976	1.032	1.088	1.117	1.146	1.098	0.973	0.912	0.822	0.759
40	0.588	0.639	0.782	0.914	1.016	1.078	1.129	1.174	1.206	1.243	1.176	1.028	0.956	0.883	0.827
$\theta = 22\frac{1}{2}^\circ$															
0	0.166	0.162	0.160	0.154	0.142	0.142	0.135	0.135	0.142	0.147	0.140	0.146	0.146	0.155	0.160
1	0.295	0.278	0.265	0.243	0.240	0.241	0.240	0.240	0.240	0.244	0.244	0.248	0.252	0.252	0.254
2	0.427	0.416	0.398	0.386	0.392	0.392	0.389	0.406	0.415	0.422	0.426	0.408	0.382	0.338	0.300
4	0.392	0.378	0.350	0.342	0.348	0.376	0.384	0.398	0.414	0.406	0.448	0.420	0.396	0.373	0.354
6	0.406	0.403	0.392	0.396	0.406	0.428	0.439	0.449	0.446	0.455	0.467	0.441	0.413	0.396	0.369
8	0.414	0.418	0.430	0.441	0.453	0.477	0.485	0.493	0.481	0.497	0.488	0.460	0.429	0.406	0.380
10	0.748	0.435	0.460	0.478	0.490	0.512	0.521	0.527	0.509	0.532	0.500	0.475	0.443	0.418	0.389
15	0.450	0.455	0.485	0.516	0.542	0.577	0.635	0.674	0.662	0.690	0.651	0.612	0.568	0.512	0.470
20	0.474	0.462	0.506	0.540	0.581	0.616	0.724	0.819	0.803	0.831	0.788	0.733	0.676	0.600	0.541
25	0.512	0.534	0.589	0.637	0.708	0.762	0.846	0.928	0.928	0.936	0.870	0.815	0.752	0.687	0.622
30	0.558	0.596	0.665	0.718	0.812	0.876	0.957	1.024	1.038	1.038	0.954	0.886	0.818	0.756	0.689
35	0.592	0.672	0.748	0.826	0.934	0.987	1.072	1.118	1.151	1.142	1.042	0.947	0.889	0.823	0.764
40	0.622	0.726	0.807	0.914	1.028	1.083	1.165	1.207	1.246	1.228	1.112	1.004	0.947	0.888	0.823
$\theta = 45^\circ$															
0	0.162	0.162	0.162	0.160	0.164	0.159	0.153	0.148	0.143	0.147	0.149	0.155	0.155	0.164	0.173
1	0.256	0.254	0.264	0.268	0.270	0.275	0.281	0.288	0.295	0.298	0.296	0.285	0.276	0.268	0.261
2	0.420	0.409	0.386	0.390	0.398	0.409	0.422	0.435	0.441	0.438	0.448	0.431	0.405	0.358	0.323
4	0.346	0.339	0.349	0.365	0.373	0.384	0.397	0.447	0.460	0.476	0.482	0.458	0.432	0.404	0.386
6	0.385	0.381	0.392	0.408	0.421	0.436	0.449	0.491	0.506	0.511	0.527	0.496	0.471	0.446	0.420
8	0.422	0.422	0.429	0.453	0.472	0.482	0.502	0.530	0.549	0.549	0.562	0.534	0.508	0.481	0.442
10	0.453	0.456	0.465	0.487	0.513	0.528	0.544	0.562	0.584	0.582	0.588	0.564	0.538	0.513	0.476
15	0.466	0.456	0.502	0.532	0.561	0.625	0.683	0.686	0.701	0.704	0.704	0.679	0.653	0.626	0.588
20	0.474	0.458	0.524	0.574	0.602	0.716	0.808	0.794	0.803	0.808	0.826	0.782	0.756	0.720	0.687
25	0.522	0.510	0.577	0.642	0.695	0.811	0.916	0.916	0.951	0.951	0.951	0.891	0.831	0.776	0.729
30	0.561	0.556	0.628	0.706	0.780	0.895	1.012	1.018	1.082	1.082	1.066	0.996	0.898	0.831	0.758
35	0.602	0.598	0.676	0.773	0.872	0.984	1.102	1.134	1.219	1.224	1.187	1.010	0.956	0.884	0.791
40	0.636	0.648	0.714	0.821	0.947	1.068	1.176	1.226	1.348	1.356	1.294	1.184	1.010	0.926	0.817

TABLE 2 (Continued)

C_J \ $\frac{r}{R}$	0.237	0.287	0.337	0.387	0.437	0.487	0.537	0.587	0.637	0.687	0.737	0.787	0.837	0.887	0.937
$\theta = 67\frac{1}{2}^\circ$															
0	0.162	0.162	0.160	0.162	0.159	0.157	0.150	0.143	0.149	0.149	0.149	0.158	0.164	0.168	0.176
1	0.274	0.282	0.290	0.300	0.307	0.307	0.312	0.315	0.318	0.315	0.321	0.318	0.314	0.306	0.294
2	0.397	0.374	0.358	0.368	0.399	0.409	0.422	0.436	0.454	0.454	0.467	0.441	0.407	0.372	0.343
4	0.364	0.375	0.390	0.406	0.426	0.458	0.487	0.504	0.512	0.516	0.494	0.470	0.449	0.415	0.400
6	0.408	0.422	0.448	0.471	0.489	0.521	0.545	0.563	0.584	0.582	0.562	0.534	0.502	0.473	0.452
8	0.451	0.469	0.507	0.529	0.553	0.579	0.608	0.617	0.652	0.651	0.634	0.596	0.557	0.528	0.506
10	0.486	0.512	0.556	0.584	0.605	0.630	0.654	0.678	0.712	0.699	0.695	0.641	0.602	0.576	0.547
15	0.495	0.521	0.558	0.596	0.651	0.708	0.762	0.796	0.870	0.867	0.820	0.773	0.711	0.651	0.602
20	0.500	0.514	0.558	0.604	0.689	0.776	0.857	0.909	1.004	1.012	0.944	0.894	0.812	0.735	0.646
25	0.541	0.541	0.603	0.659	0.758	0.862	0.958	1.022	1.115	1.109	1.075	1.012	0.906	0.809	0.718
30	0.572	0.568	0.641	0.712	0.821	0.943	1.042	1.116	1.216	1.198	1.206	1.118	0.985	0.876	0.790
35	0.609	0.593	0.685	0.763	0.887	1.019	1.126	1.218	1.319	1.284	1.321	1.235	1.071	0.942	0.862
40	0.637	0.612	0.726	0.808	0.942	1.096	1.207	1.302	1.409	1.376	1.418	1.326	1.148	1.004	0.926
$\theta = 90^\circ$															
0	0.166	0.162	0.162	0.162	0.162	0.154	0.154	0.157	0.150	0.150	0.162	0.162	0.165	0.168	0.176
1	0.307	0.314	0.326	0.326	0.326	0.330	0.332	0.338	0.346	0.346	0.348	0.352	0.342	0.334	0.308
2	0.374	0.365	0.358	0.374	0.402	0.442	0.456	0.502	0.483	0.514	0.480	0.448	0.431	0.402	0.381
4	0.406	0.410	0.427	0.446	0.463	0.475	0.498	0.512	0.520	0.514	0.527	0.506	0.478	0.446	0.432
6	0.442	0.448	0.498	0.523	0.529	0.546	0.554	0.586	0.590	0.590	0.588	0.562	0.543	0.511	0.487
8	0.483	0.479	0.546	0.584	0.593	0.612	0.621	0.664	0.664	0.664	0.645	0.618	0.598	0.565	0.541
10	0.516	0.522	0.584	0.627	0.644	0.672	0.689	0.726	0.713	0.719	0.684	0.669	0.658	0.627	0.594
15	0.522	0.522	0.588	0.634	0.682	0.741	0.794	0.861	0.870	0.874	0.832	0.798	0.763	0.728	0.675
20	0.522	0.514	0.576	0.638	0.716	0.804	0.896	0.975	1.016	1.035	0.997	0.926	0.864	0.816	0.749
25	0.549	0.542	0.610	0.686	0.769	0.881	0.974	1.048	1.129	1.142	1.106	1.034	0.980	0.891	0.823
30	0.574	0.566	0.641	0.732	0.814	0.932	1.048	1.109	1.218	1.239	1.228	1.127	1.072	0.972	0.896
35	0.591	0.589	0.670	0.776	0.866	0.987	1.116	1.214	1.314	1.327	1.331	1.228	1.166	1.059	0.972
40	0.605	0.605	0.694	0.811	0.909	1.048	1.188	1.302	1.409	1.402	1.426	1.314	1.246	1.127	1.034
$\theta = 112\frac{1}{2}^\circ$															
0	0.164	0.164	0.162	0.162	0.160	0.164	0.158	0.158	0.160	0.162	0.158	0.160	0.164	0.170	0.179
1	0.318	0.318	0.326	0.334	0.334	0.334	0.330	0.336	0.340	0.348	0.348	0.344	0.331	0.326	0.304
2	0.396	0.374	0.374	0.388	0.406	0.454	0.482	0.508	0.511	0.504	0.514	0.483	0.442	0.400	0.361
4	0.433	0.421	0.428	0.445	0.468	0.489	0.496	0.522	0.543	0.531	0.550	0.526	0.509	0.495	0.448
6	0.471	0.464	0.483	0.518	0.536	0.554	0.572	0.598	0.602	0.602	0.602	0.572	0.554	0.542	0.492
8	0.489	0.489	0.526	0.592	0.598	0.622	0.647	0.651	0.658	0.667	0.654	0.635	0.608	0.584	0.554
10	0.500	0.522	0.596	0.627	0.651	0.684	0.718	0.720	0.710	0.725	0.693	0.673	0.648	0.621	0.596
15	0.518	0.518	0.578	0.642	0.715	0.792	0.846	0.882	0.886	0.891	0.857	0.811	0.754	0.715	0.662
20	0.514	0.510	0.543	0.678	0.784	0.886	0.952	1.018	1.038	1.063	1.008	0.932	0.845	0.796	0.749
25	0.536	0.543	0.612	0.719	0.827	0.947	1.022	1.106	1.136	1.151	1.126	1.029	0.968	0.904	0.846
30	0.558	0.582	0.645	0.756	0.859	0.994	1.089	1.194	1.219	1.237	1.210	1.116	1.063	0.992	0.931
35	0.582	0.629	0.682	0.787	0.897	1.052	1.157	1.298	1.322	1.331	1.331	1.228	1.158	1.088	1.024
40	0.594	0.653	0.726	0.815	0.933	1.100	1.224	1.389	1.425	1.413	1.436	1.315	1.243	1.180	1.096

TABLE 2 (Continued)

$\frac{r}{R}$	0.237	0.287	0.337	0.387	0.437	0.487	0.537	0.587	0.637	0.687	0.737	0.787	0.837	0.887	0.937
C_J															
$\theta = 135^\circ$															
0	0.164	0.164	0.164	0.160	0.158	0.158	0.160	0.164	0.162	0.164	0.164	0.168	0.172	0.176	0.184
1	0.318	0.316	0.320	0.320	0.325	0.328	0.331	0.331	0.331	0.336	0.336	0.332	0.318	0.314	0.304
2	0.400	0.368	0.354	0.385	0.402	0.461	0.503	0.526	0.530	0.524	0.481	0.454	0.416	0.388	0.354
4	0.418	0.412	0.416	0.432	0.449	0.465	0.484	0.494	0.523	0.538	0.534	0.526	0.518	0.509	0.506
6	0.425	0.437	0.462	0.496	0.512	0.537	0.562	0.571	0.567	0.602	0.598	0.584	0.564	0.546	0.529
8	0.439	0.476	0.507	0.561	0.578	0.604	0.638	0.642	0.628	0.667	0.654	0.641	0.611	0.590	0.563
10	0.457	0.503	0.548	0.604	0.633	0.668	0.700	0.700	0.598	0.714	0.702	0.685	0.653	0.621	0.589
15	0.472	0.509	0.548	0.612	0.691	0.779	0.856	0.882	0.875	0.925	0.882	0.807	0.742	0.712	0.674
20	0.484	0.498	0.556	0.627	0.734	0.876	0.994	1.059	1.100	1.128	1.010	0.914	0.826	0.784	0.753
25	0.506	0.532	0.594	0.682	0.802	0.952	1.074	1.150	1.193	1.216	1.121	1.038	0.954	0.896	0.862
30	0.529	0.576	0.641	0.721	0.862	1.024	1.152	1.236	1.274	1.279	1.228	1.146	1.062	0.992	0.941
35	0.553	0.614	0.678	0.768	0.927	1.107	1.234	1.324	1.358	1.354	1.337	1.259	1.178	1.081	1.040
40	0.574	0.643	0.715	0.805	0.986	1.183	1.289	1.407	1.421	1.410	1.425	1.363	1.287	1.198	1.121
$\theta = 167\frac{1}{2}^\circ$															
0	0.162	0.162	0.162	0.164	0.164	0.160	0.158	0.158	0.160	0.162	0.160	0.164	0.168	0.170	0.177
1	0.318	0.320	0.320	0.316	0.322	0.322	0.322	0.328	0.328	0.328	0.334	0.328	0.316	0.309	0.269
2	0.400	0.362	0.365	0.380	0.406	0.430	0.468	0.502	0.508	0.524	0.514	0.473	0.421	0.375	0.346
4	0.393	0.409	0.423	0.431	0.438	0.452	0.474	0.491	0.504	0.509	0.536	0.530	0.521	0.514	0.512
6	0.411	0.438	0.467	0.492	0.512	0.527	0.548	0.571	0.574	0.582	0.602	0.592	0.579	0.561	0.546
8	0.430	0.469	0.504	0.557	0.585	0.596	0.611	0.654	0.648	0.648	0.684	0.650	0.637	0.623	0.585
10	0.448	0.494	0.542	0.612	0.646	0.663	0.689	0.721	0.718	0.712	0.734	0.702	0.682	0.660	0.614
15	0.458	0.503	0.548	0.625	0.721	0.788	0.852	0.896	0.912	0.912	0.912	0.846	0.807	0.714	0.691
20	0.466	0.494	0.552	0.634	0.800	0.906	1.004	1.068	1.114	1.118	1.084	0.962	0.904	0.756	0.756
25	0.485	0.523	0.596	0.679	0.863	0.984	1.092	1.172	1.216	1.241	1.226	1.115	1.035	0.882	0.831
30	0.503	0.548	0.631	0.722	0.915	1.057	1.174	1.276	1.309	1.336	1.376	1.207	1.112	1.000	0.907
35	0.520	0.579	0.666	0.771	0.968	1.135	1.258	1.368	1.398	1.442	1.463	1.326	1.229	1.146	1.026
40	0.532	0.601	0.694	0.802	1.002	1.208	1.324	1.462	1.497	1.554	1.541	1.416	1.338	1.278	1.174
$\theta = 180^\circ$															
0	0.160	0.160	0.160	0.160	0.160	0.158	0.156	0.156	0.162	0.165	0.160	0.160	0.166	0.168	0.175
1	0.326	0.326	0.334	0.338	0.338	0.334	0.340	0.346	0.342	0.334	0.326	0.318	0.304	0.294	0.258
2	0.411	0.384	0.373	0.395	0.413	0.442	0.466	0.489	0.510	0.514	0.530	0.492	0.411	0.363	0.325
4	0.384	0.411	0.418	0.432	0.446	0.455	0.462	0.476	0.488	0.500	0.514	0.523	0.520	0.508	0.510
6	0.402	0.433	0.453	0.478	0.512	0.526	0.531	0.554	0.562	0.576	0.592	0.586	0.583	0.564	0.558
8	0.423	0.441	0.489	0.544	0.578	0.598	0.615	0.637	0.641	0.655	0.668	0.654	0.651	0.618	0.604
10	0.435	0.469	0.524	0.610	0.635	0.662	0.689	0.706	0.715	0.721	0.738	0.715	0.702	0.667	0.642
15	0.446	0.460	0.528	0.600	0.718	0.786	0.802	0.894	0.894	0.918	0.918	0.886	0.860	0.735	0.697
20	0.451	0.460	0.530	0.607	0.794	0.903	1.000	1.086	1.086	1.109	1.084	1.048	1.002	0.800	0.743
25	0.462	0.489	0.564	0.662	0.842	0.984	1.125	1.160	1.167	1.248	1.202	1.166	1.122	0.951	0.876
30	0.469	0.517	0.600	0.716	0.887	1.042	1.206	1.217	1.225	1.364	1.336	1.279	1.228	1.082	0.991
35	0.478	0.544	0.641	0.774	0.934	1.117	1.295	1.360	1.366	1.512	1.476	1.394	1.331	1.212	1.128
40	0.485	0.568	0.663	0.805	0.966	1.169	1.381	1.524	1.528	1.631	1.599	1.502	1.426	1.334	1.242

TABLE 3 BASE SUCTION COEFFICIENTS 10° INCIDENCE

$\frac{r}{R}$	0.237	0.287	0.337	0.387	0.437	0.487	0.537	0.587	0.637	0.687	0.737	0.787	0.837	0.887	0.937
C_J															
$\theta = 0°$															
0	0.156	0.154	0.158	0.154	0.154	0.156	0.158	0.160	0.162	0.162	0.162	0.165	0.165	0.173	0.186
1	0.264	0.245	0.215	0.196	0.183	0.178	0.168	0.159	0.156	0.156	0.162	0.168	0.160	0.154	0.156
2	0.430	0.421	0.416	0.404	0.386	0.374	0.370	0.363	0.361	0.363	0.363	0.365	0.348	0.332	0.326
4	0.468	0.446	0.438	0.434	0.438	0.441	0.448	0.456	0.462	0.464	0.470	0.473	0.456	0.442	0.430
6	0.504	0.471	0.459	0.459	0.456	0.448	0.442	0.448	0.472	0.468	0.468	0.470	0.462	0.440	0.432
8	0.536	0.493	0.478	0.473	0.468	0.465	0.446	0.452	0.468	0.475	0.472	0.462	0.454	0.446	0.439
10	0.561	0.510	0.494	0.486	0.465	0.443	0.436	0.452	0.462	0.466	0.468	0.462	0.456	0.448	0.442
15	0.578	0.552	0.542	0.538	0.552	0.561	0.598	0.615	0.675	0.659	0.609	0.571	0.518	0.473	0.457
20	0.592	0.580	0.584	0.596	0.631	0.674	0.726	0.798	0.858	0.806	0.722	0.640	0.563	0.511	0.468
25	0.642	0.642	0.651	0.680	0.736	0.817	0.864	0.894	0.941	0.903	0.817	0.732	0.667	0.609	0.556
30	0.716	0.687	0.706	0.771	0.824	0.926	0.998	0.986	1.022	0.964	0.903	0.829	0.742	0.693	0.636
35	0.787	0.741	0.769	0.857	0.918	1.058	1.116	1.108	1.095	1.039	0.971	0.906	0.839	0.786	0.712
40	0.835	0.796	0.824	0.932	1.006	1.173	1.225	1.194	1.154	1.102	1.064	1.000	0.935	0.861	0.793
$\theta = 22\frac{1}{2}°$															
0	0.150	0.142	0.142	0.146	0.146	0.146	0.152	0.156	0.156	0.160	0.162	0.174	0.188	0.206	0.223
1	0.326	0.294	0.276	0.253	0.238	0.215	0.200	0.187	0.187	0.198	0.214	0.221	0.205	0.196	0.193
2	0.458	0.443	0.428	0.419	0.410	0.406	0.400	0.403	0.410	0.414	0.418	0.412	0.400	0.378	0.356
4	0.488	0.474	0.465	0.450	0.448	0.448	0.463	0.468	0.482	0.500	0.513	0.502	0.478	0.443	0.430
6	0.520	0.506	0.486	0.468	0.459	0.456	0.476	0.479	0.483	0.506	0.508	0.506	0.482	0.448	0.436
8	0.565	0.544	0.505	0.483	0.475	0.475	0.485	0.489	0.496	0.514	0.514	0.510	0.486	0.461	0.448
10	0.621	0.576	0.513	0.492	0.486	0.480	0.493	0.496	0.513	0.528	0.532	0.518	0.503	0.466	0.444
15	0.618	0.602	0.558	0.556	0.599	0.637	0.662	0.689	0.706	0.706	0.664	0.610	0.547	0.510	0.465
20	0.584	0.586	0.592	0.615	0.695	0.778	0.814	0.893	0.921	0.875	0.786	0.692	0.584	0.540	0.481
25	0.652	0.654	0.661	0.723	0.802	0.895	0.952	1.018	1.024	0.956	0.881	0.786	0.718	0.643	0.569
30	0.696	0.696	0.722	0.816	0.898	1.006	1.074	1.135	1.118	1.028	0.962	0.891	0.847	0.738	0.647
35	0.750	0.739	0.803	0.908	1.004	1.121	1.206	1.254	1.186	1.102	1.046	0.985	0.936	0.835	0.731
40	0.812	0.787	0.864	0.987	1.086	1.224	1.315	1.352	1.209	1.154	1.113	1.068	1.013	0.926	0.808
$\theta = 45°$															
0	0.156	0.156	0.150	0.154	0.156	0.156	0.160	0.162	0.165	0.168	0.173	0.180	0.194	0.206	0.221
1	0.394	0.358	0.339	0.304	0.283	0.267	0.259	0.263	0.285	0.308	0.312	0.305	0.283	0.255	0.231
2	0.493	0.471	0.458	0.442	0.438	0.431	0.425	0.425	0.441	0.446	0.443	0.436	0.431	0.418	0.400
4	0.526	0.531	0.535	0.535	0.538	0.540	0.546	0.546	0.548	0.551	0.555	0.558	0.553	0.551	0.542
6	0.584	0.576	0.561	0.556	0.559	0.559	0.568	0.564	0.572	0.580	0.586	0.583	0.571	0.560	0.548
8	0.642	0.615	0.586	0.580	0.585	0.580	0.586	0.590	0.598	0.609	0.621	0.604	0.593	0.572	0.564
10	0.694	0.642	0.608	0.598	0.594	0.596	0.600	0.611	0.626	0.633	0.642	0.636	0.614	0.594	0.573
15	0.752	0.716	0.689	0.679	0.679	0.706	0.744	0.762	0.835	0.894	0.824	0.753	0.695	0.656	0.596
20	0.804	0.780	0.764	0.760	0.768	0.804	0.862	0.935	1.020	1.102	1.000	0.884	0.771	0.708	0.621
25	0.838	0.808	0.804	0.802	0.851	0.916	0.978	1.057	1.146	1.186	1.076	0.961	0.865	0.796	0.752
30	0.869	0.832	0.840	0.856	0.938	1.022	1.085	1.174	1.237	1.258	1.138	1.032	0.956	0.882	0.834
35	0.895	0.857	0.876	0.922	1.019	1.119	1.186	1.298	1.340	1.329	1.190	1.089	1.044	0.978	0.930
40	0.923	0.876	0.914	1.004	1.095	1.213	1.294	1.412	1.423	1.384	1.224	1.166	1.122	1.065	1.018

TABLE 3 (Continued)

$\frac{r}{R}$	0.237	0.287	0.337	0.387	0.437	0.487	0.537	0.587	0.637	0.687	0.737	0.787	0.837	0.887	0.937
C_J															
$\theta = 67\frac{1}{2}^\circ$															
0	0.158	0.158	0.156	0.158	0.160	0.160	0.163	0.167	0.172	0.179	0.183	0.186	0.193	0.211	0.237
1	0.404	0.386	0.354	0.321	0.303	0.284	0.292	0.326	0.360	0.401	0.406	0.373	0.346	0.314	0.294
2	0.488	0.471	0.450	0.424	0.428	0.453	0.471	0.497	0.504	0.493	0.495	0.475	0.469	0.454	0.448
4	0.559	0.562	0.566	0.573	0.576	0.573	0.573	0.574	0.578	0.589	0.608	0.602	0.585	0.578	0.563
6	0.614	0.607	0.592	0.592	0.605	0.608	0.610	0.612	0.618	0.622	0.629	0.627	0.602	0.596	0.579
8	0.668	0.645	0.620	0.615	0.627	0.635	0.642	0.657	0.655	0.655	0.661	0.654	0.630	0.621	0.591
10	0.713	0.669	0.643	0.637	0.644	0.659	0.671	0.692	0.688	0.679	0.688	0.679	0.666	0.648	0.603
15	0.762	0.731	0.688	0.685	0.702	0.736	0.794	0.845	0.859	0.848	0.856	0.834	0.789	0.732	0.692
20	0.805	0.748	0.714	0.738	0.776	0.825	0.902	1.014	1.018	1.023	1.039	1.006	0.934	0.846	0.800
25	0.843	0.814	0.785	0.805	0.854	0.921	1.004	1.092	1.131	1.128	1.148	1.110	1.029	0.941	0.886
30	0.876	0.847	0.837	0.862	0.931	1.004	1.096	1.156	1.234	1.234	1.254	1.198	1.112	1.022	0.952
35	0.985	0.864	0.892	0.946	1.012	1.089	1.182	1.221	1.338	1.341	1.344	1.306	1.204	1.112	1.038
40	0.913	0.886	0.943	1.000	1.084	1.188	1.274	1.389	1.423	1.423	1.441	1.404	1.296	1.183	1.102
$\theta = 90^\circ$															
0	0.158	0.158	0.160	0.160	0.160	0.163	0.167	0.172	0.175	0.182	0.185	0.196	0.214	0.231	0.256
1	0.404	0.387	0.372	0.341	0.333	0.325	0.346	0.358	0.372	0.405	0.416	0.426	0.418	0.396	0.373
2	0.486	0.474	0.460	0.442	0.447	0.461	0.492	0.516	0.534	0.552	0.554	0.538	0.509	0.482	0.467
4	0.545	0.567	0.584	0.608	0.614	0.592	0.586	0.592	0.603	0.616	0.625	0.619	0.610	0.600	0.588
6	0.596	0.596	0.602	0.622	0.631	0.629	0.629	0.621	0.628	0.642	0.652	0.658	0.642	0.628	0.614
8	0.649	0.631	0.626	0.638	0.645	0.654	0.671	0.662	0.662	0.678	0.689	0.689	0.668	0.652	0.639
10	0.682	0.654	0.641	0.646	0.651	0.692	0.714	0.684	0.689	0.705	0.723	0.716	0.704	0.689	0.661
15	0.727	0.711	0.698	0.688	0.712	0.775	0.837	0.865	0.847	0.877	0.988	0.988	0.892	0.830	0.772
20	0.774	0.758	0.740	0.727	0.760	0.841	0.953	1.034	1.008	1.038	1.142	1.136	1.066	0.984	0.896
25	0.796	0.782	0.782	0.789	0.822	0.934	1.047	1.139	1.145	1.185	1.261	1.245	1.162	1.056	0.967
30	0.812	0.809	0.815	0.851	0.896	0.973	1.136	1.228	1.267	1.312	1.356	1.341	1.256	1.127	1.043
35	0.826	0.834	0.844	0.916	0.954	1.102	1.228	1.326	1.380	1.460	1.472	1.468	1.338	1.204	1.105
40	0.847	0.862	0.871	0.964	1.027	1.198	1.311	1.409	1.493	1.568	1.587	1.564	1.423	1.288	1.172
$\theta = 112\frac{1}{2}^\circ$															
0	0.158	0.160	0.158	0.162	0.162	0.168	0.173	0.176	0.184	0.184	0.192	0.198	0.202	0.219	0.244
1	0.389	0.384	0.376	0.364	0.359	0.365	0.374	0.385	0.403	0.414	0.425	0.428	0.418	0.398	0.370
2	0.513	0.483	0.454	0.443	0.451	0.467	0.478	0.493	0.511	0.526	0.541	0.556	0.558	0.548	0.531
4	0.538	0.552	0.568	0.581	0.598	0.612	0.593	0.585	0.604	0.626	0.631	0.620	0.614	0.605	0.602
6	0.576	0.574	0.589	0.605	0.627	0.645	0.628	0.628	0.641	0.652	0.668	0.651	0.642	0.630	0.614
8	0.608	0.608	0.608	0.632	0.654	0.678	0.663	0.665	0.674	0.685	0.702	0.680	0.670	0.664	0.635
10	0.643	0.630	0.632	0.654	0.678	0.704	0.695	0.700	0.706	0.712	0.729	0.714	0.702	0.684	0.642
15	0.617	0.617	0.647	0.697	0.742	0.809	0.842	0.882	0.928	0.959	0.959	0.916	0.881	0.850	0.785
20	0.605	0.602	0.658	0.735	0.813	0.902	1.010	1.057	1.126	1.174	1.188	1.102	1.057	1.026	0.924
25	0.656	0.652	0.697	0.775	0.874	0.987	1.131	1.166	1.248	1.293	1.307	1.256	1.174	1.112	1.009
30	0.708	0.710	0.726	0.812	0.928	1.068	1.228	1.254	1.371	1.395	1.432	1.380	1.288	1.190	1.078
35	0.779	0.772	0.760	0.857	0.980	1.156	1.320	1.334	1.493	1.516	1.570	1.509	1.406	1.289	1.153
40	0.825	0.814	0.808	0.894	1.016	1.224	1.402	1.423	1.605	1.622	1.684	1.632	1.521	1.365	1.204

TABLE 3 (Continued)

$\frac{r}{R}$	0.237	0.287	0.337	0.387	0.437	0.487	0.537	0.587	0.637	0.687	0.737	0.787	0.837	0.887	0.937
C_J															
$\theta = 135^\circ$															
0	0.162	0.162	0.160	0.160	0.162	0.167	0.172	0.175	0.178	0.184	0.184	0.190	0.195	0.206	0.216
1	0.400	0.391	0.386	0.386	0.384	0.384	0.391	0.416	0.416	0.418	0.427	0.412	0.384	0.349	0.326
2	0.524	0.502	0.482	0.459	0.463	0.473	0.489	0.496	0.508	0.526	0.540	0.543	0.519	0.502	0.484
4	0.534	0.546	0.558	0.572	0.586	0.605	0.594	0.589	0.600	0.614	0.638	0.646	0.638	0.622	0.614
6	0.560	0.564	0.584	0.600	0.624	0.639	0.631	0.629	0.636	0.652	0.675	0.667	0.660	0.645	0.632
8	0.589	0.589	0.609	0.631	0.659	0.678	0.668	0.668	0.671	0.686	0.708	0.694	0.685	0.672	0.657
10	0.614	0.622	0.631	0.654	0.688	0.712	0.692	0.706	0.710	0.715	0.736	0.718	0.704	0.691	0.672
15	0.578	0.581	0.592	0.637	0.721	0.820	0.856	0.930	0.996	0.996	1.025	0.967	0.916	0.872	0.815
20	0.522	0.556	0.590	0.674	0.786	0.911	1.032	1.164	1.284	1.280	1.304	1.222	1.138	1.046	0.963
25	0.609	0.612	0.647	0.680	0.852	0.980	1.164	1.260	1.396	1.412	1.428	1.346	1.250	1.132	1.038
30	0.681	0.674	0.691	0.778	0.916	1.064	1.238	1.356	1.491	1.554	1.537	1.450	1.376	1.224	1.112
35	0.776	0.754	0.756	0.830	0.970	1.121	1.332	1.444	1.590	1.681	1.642	1.572	1.498	1.302	1.196
40	0.828	0.804	0.804	0.898	1.002	1.109	1.413	1.537	1.687	1.802	1.743	1.684	1.613	1.389	1.268
$\theta = 167\frac{1}{2}^\circ$															
0	0.162	0.162	0.162	0.162	0.162	0.165	0.168	0.172	0.175	0.175	0.179	0.186	0.193	0.204	0.212
1	0.406	0.394	0.384	0.386	0.389	0.396	0.412	0.415	0.418	0.423	0.420	0.400	0.362	0.309	0.274
2	0.542	0.522	0.506	0.487	0.476	0.476	0.482	0.496	0.514	0.526	0.520	0.508	0.488	0.469	0.454
4	0.528	0.540	0.553	0.576	0.589	0.613	0.628	0.606	0.589	0.614	0.648	0.641	0.633	0.620	0.615
6	0.554	0.564	0.589	0.609	0.621	0.649	0.657	0.638	0.642	0.652	0.675	0.668	0.654	0.641	0.632
8	0.579	0.598	0.622	0.635	0.657	0.678	0.678	0.664	0.681	0.691	0.711	0.692	0.681	0.669	0.657
10	0.592	0.626	0.647	0.664	0.688	0.716	0.696	0.692	0.714	0.720	0.736	0.718	0.708	0.692	0.674
15	0.574	0.578	0.591	0.674	0.759	0.859	0.918	0.950	1.035	1.059	1.068	0.986	0.936	0.925	0.847
20	0.506	0.543	0.582	0.674	0.824	1.002	1.146	1.224	1.318	1.416	1.388	1.258	1.185	1.116	1.023
25	0.549	0.588	0.673	0.738	0.875	1.087	1.227	1.376	1.456	1.545	1.534	1.376	1.292	1.192	1.092
30	0.615	0.639	0.716	0.793	0.912	1.162	1.311	1.501	1.625	1.668	1.662	1.489	1.406	1.289	1.178
35	0.673	0.721	0.770	0.837	0.958	1.246	1.415	1.650	1.716	1.779	1.748	1.592	1.511	1.362	1.276
40	0.728	0.808	0.824	0.885	0.996	1.310	1.509	1.784	1.902	1.882	1.845	1.714	1.600	1.448	1.356
$\theta = 180^\circ$															
0	0.158	0.156	0.162	0.160	0.160	0.163	0.172	0.170	0.172	0.176	0.176	0.184	0.192	0.190	0.204
1	0.412	0.398	0.394	0.388	0.392	0.395	0.406	0.418	0.423	0.426	0.409	0.384	0.304	0.278	0.256
2	0.544	0.538	0.520	0.500	0.484	0.482	0.488	0.496	0.508	0.515	0.520	0.510	0.482	0.470	0.453
4	0.528	0.546	0.556	0.582	0.594	0.608	0.618	0.631	0.640	0.634	0.646	0.648	0.634	0.621	0.610
6	0.556	0.565	0.584	0.613	0.629	0.649	0.642	0.659	0.662	0.662	0.683	0.678	0.664	0.643	0.627
8	0.573	0.594	0.629	0.648	0.674	0.675	0.665	0.671	0.694	0.706	0.711	0.694	0.682	0.665	0.649
10	0.582	0.621	0.668	0.692	0.708	0.703	0.686	0.692	0.714	0.722	0.718	0.718	0.710	0.704	0.686
15	0.567	0.596	0.642	0.674	0.786	0.911	0.927	0.884	0.965	1.018	1.024	1.006	0.943	0.918	0.837
20	0.481	0.522	0.578	0.680	0.852	1.022	1.181	1.271	1.280	1.296	1.356	1.287	1.214	1.122	1.044
25	0.542	0.573	0.615	0.724	0.896	1.089	1.265	1.376	1.426	1.452	1.514	1.439	1.328	1.248	1.135
30	0.586	0.608	0.659	0.785	0.941	1.144	1.328	1.460	1.590	1.604	1.670	1.578	1.446	1.352	1.216
35	0.620	0.634	0.692	0.831	0.986	1.201	1.442	1.568	1.728	1.778	1.852	1.723	1.574	1.446	1.309
40	0.644	0.676	0.737	0.860	1.022	1.243	1.450	1.654	1.871	1.920	2.003	1.845	1.682	1.520	1.382

TABLE 4 BASE SUCTION COEFFICIENTS 15° INCIDENCE

$\frac{r}{R}$	0.237	0.287	0.337	0.387	0.437	0.487	0.537	0.587	0.637	0.687	0.737	0.787	0.837	0.887	0.937
C_J															
$\theta = 0°$															
0	0.158	0.158	0.158	0.156	0.154	0.158	0.158	0.160	0.162	0.166	0.171	0.185	0.193	0.202	0.216
1	0.318	0.296	0.273	0.259	0.246	0.239	0.228	0.235	0.239	0.242	0.248	0.226	0.198	0.196	0.185
2	0.508	0.489	0.485	0.468	0.461	0.453	0.432	0.428	0.426	0.413	0.404	0.392	0.381	0.365	0.355
4	0.576	0.564	0.550	0.531	0.514	0.496	0.475	0.446	0.438	0.427	0.420	0.415	0.408	0.400	0.391
6	0.647	0.608	0.591	0.559	0.538	0.517	0.498	0.470	0.456	0.442	0.436	0.424	0.419	0.394	0.386
8	0.703	0.657	0.628	0.592	0.575	0.539	0.521	0.496	0.472	0.451	0.448	0.429	0.419	0.403	0.393
10	0.764	0.698	0.654	0.586	0.569	0.556	0.539	0.504	0.488	0.463	0.454	0.431	0.408	0.396	0.393
15	0.682	0.584	0.475	0.546	0.580	0.585	0.583	0.569	0.556	0.540	0.529	0.498	0.467	0.420	0.384
20	0.513	0.396	0.394	0.492	0.584	0.607	0.619	0.623	0.623	0.615	0.602	0.546	0.495	0.416	0.375
25	0.586	0.472	0.472	0.548	0.714	0.762	0.792	0.792	0.785	0.725	0.691	0.618	0.556	0.486	0.436
30	0.639	0.562	0.565	0.632	0.820	0.931	0.936	0.934	0.924	0.819	0.762	0.681	0.600	0.541	0.520
35	0.698	0.640	0.668	0.776	0.948	1.085	1.092	1.079	1.076	0.925	0.840	0.740	0.668	0.612	0.576
40	0.743	0.726	0.784	0.903	1.105	1.224	1.248	1.239	1.204	1.037	0.908	0.786	0.714	0.676	0.612
$\theta = 22\frac{1}{2}°$															
0	0.158	0.160	0.160	0.158	0.158	0.160	0.160	0.162	0.168	0.176	0.184	0.191	0.195	0.206	0.221
1	0.319	0.302	0.288	0.280	0.280	0.288	0.294	0.290	0.296	0.300	0.296	0.285	0.263	0.232	0.213
2	0.524	0.508	0.496	0.485	0.482	0.473	0.468	0.460	0.456	0.448	0.431	0.427	0.414	0.400	0.392
4	0.593	0.584	0.571	0.556	0.541	0.528	0.511	0.495	0.472	0.472	0.468	0.459	0.450	0.442	0.430
6	0.638	0.632	0.625	0.602	0.576	0.561	0.539	0.526	0.506	0.499	0.491	0.477	0.472	0.455	0.437
8	0.695	0.680	0.671	0.647	0.620	0.589	0.566	0.548	0.538	0.526	0.515	0.502	0.485	0.467	0.432
10	0.754	0.736	0.710	0.684	0.652	0.615	0.589	0.573	0.561	0.548	0.531	0.520	0.500	0.481	0.426
15	0.776	0.742	0.725	0.686	0.640	0.627	0.625	0.620	0.622	0.625	0.617	0.589	0.564	0.537	0.489
20	0.804	0.631	0.542	0.558	0.621	0.642	0.658	0.671	0.692	0.684	0.706	0.652	0.623	0.583	0.554
25	0.816	0.685	0.636	0.629	0.760	0.776	0.832	0.891	0.876	0.822	0.802	0.737	0.697	0.645	0.596
30	0.825	0.728	0.702	0.753	0.905	0.948	1.005	1.098	1.065	0.941	0.889	0.810	0.758	0.698	0.639
35	0.831	0.743	0.771	0.885	1.018	1.095	1.162	1.261	1.231	1.074	0.987	0.885	0.823	0.753	0.682
40	0.828	0.756	0.823	1.014	1.125	1.226	1.314	1.406	1.382	1.194	1.073	0.956	0.882	0.804	0.723
$\theta = 45°$															
0	0.156	0.156	0.158	0.154	0.158	0.160	0.158	0.162	0.168	0.176	0.186	0.198	0.206	0.228	0.244
1	0.354	0.346	0.331	0.315	0.311	0.354	0.382	0.416	0.412	0.418	0.428	0.402	0.375	0.334	0.308
2	0.536	0.528	0.524	0.516	0.510	0.502	0.496	0.483	0.471	0.498	0.510	0.502	0.493	0.488	0.476
4	0.608	0.613	0.618	0.624	0.616	0.604	0.589	0.571	0.542	0.528	0.520	0.524	0.536	0.521	0.511
6	0.658	0.658	0.658	0.658	0.658	0.649	0.641	0.635	0.621	0.596	0.589	0.584	0.578	0.559	0.545
8	0.702	0.700	0.695	0.695	0.689	0.694	0.687	0.693	0.687	0.662	0.647	0.638	0.620	0.592	0.578
10	0.750	0.742	0.730	0.724	0.731	0.738	0.740	0.746	0.742	0.728	0.712	0.694	0.662	0.624	0.608
15	0.894	0.793	0.762	0.752	0.768	0.792	0.816	0.830	0.839	0.839	0.837	0.815	0.780	0.741	0.713
20	1.029	0.824	0.786	0.794	0.802	0.839	0.885	0.921	0.928	0.936	0.954	0.926	0.884	0.845	0.812
25	1.096	0.951	0.895	0.889	0.906	0.952	1.021	1.068	1.052	1.049	1.085	1.051	1.006	0.937	0.884
30	1.158	1.067	0.984	0.976	0.995	1.064	1.149	1.194	1.167	1.167	1.209	1.164	1.100	1.026	0.966
35	1.215	1.185	1.089	1.069	1.089	1.179	1.284	1.335	1.295	1.270	1.326	1.278	1.211	1.115	1.032
40	1.284	1.284	1.178	1.156	1.184	1.290	1.400	1.456	1.402	1.374	1.442	1.382	1.304	1.198	1.103

TABLE 4 (Continued)

$\frac{r}{R}$	0.237	0.287	0.337	0.387	0.437	0.487	0.537	0.587	0.637	0.687	0.737	0.787	0.837	0.887	0.937
C_J															
$\theta = 67\frac{1}{2}^\circ$															
0	0.158	0.160	0.160	0.162	0.162	0.165	0.184	0.192	0.204	0.221	0.236	0.248	0.253	0.265	0.281
1	0.367	0.352	0.349	0.352	0.364	0.389	0.409	0.413	0.418	0.424	0.416	0.408	0.387	0.376	0.347
2	0.548	0.546	0.543	0.543	0.546	0.542	0.521	0.514	0.508	0.508	0.519	0.532	0.521	0.512	0.500
4	0.556	0.592	0.614	0.624	0.635	0.628	0.617	0.608	0.602	0.584	0.576	0.589	0.600	0.613	0.598
6	0.602	0.630	0.651	0.662	0.672	0.672	0.668	0.654	0.658	0.662	0.639	0.641	0.638	0.630	0.625
8	0.643	0.675	0.698	0.695	0.711	0.711	0.723	0.712	0.716	0.721	0.714	0.689	0.682	0.675	0.661
10	0.680	0.713	0.724	0.736	0.745	0.756	0.761	0.758	0.763	0.765	0.765	0.752	0.736	0.728	0.717
15	0.847	0.798	0.835	0.824	0.839	0.861	0.889	0.906	0.928	0.925	0.912	0.910	0.882	0.865	0.848
20	1.026	0.973	0.954	0.905	0.927	0.955	1.008	1.049	1.063	1.058	1.076	1.054	1.028	1.012	1.002
25	1.219	1.119	1.028	0.971	0.991	1.062	1.120	1.182	1.225	1.188	1.214	1.193	1.175	1.130	1.112
30	1.408	1.258	1.093	1.028	1.063	1.167	1.228	1.315	1.358	1.310	1.325	1.320	1.300	1.261	1.204
35	1.589	1.341	1.155	1.089	1.139	1.265	1.319	1.446	1.496	1.448	1.448	1.436	1.442	1.378	1.309
40	1.765	1.432	1.227	1.154	1.208	1.354	1.412	1.574	1.621	1.573	1.564	1.618	1.586	1.493	1.382
$\theta = 90^\circ$															
0	0.158	0.160	0.162	0.162	0.165	0.178	0.191	0.203	0.218	0.245	0.254	0.269	0.276	0.280	0.287
1	0.382	0.374	0.368	0.378	0.382	0.392	0.416	0.416	0.424	0.430	0.442	0.461	0.433	0.412	0.390
2	0.542	0.544	0.544	0.536	0.536	0.538	0.542	0.534	0.528	0.536	0.541	0.558	0.552	0.534	0.509
4	0.548	0.561	0.592	0.613	0.638	0.631	0.628	0.625	0.628	0.616	0.593	0.589	0.611	0.618	0.598
6	0.589	0.610	0.630	0.655	0.675	0.671	0.671	0.678	0.178	0.662	0.654	0.643	0.658	0.652	0.635
8	0.624	0.665	0.675	0.692	0.712	0.712	0.716	0.732	0.716	0.716	0.716	0.710	0.705	0.705	0.687
10	0.676	0.708	0.716	0.734	0.752	0.758	0.763	0.770	0.763	0.765	0.776	0.768	0.762	0.751	0.743
15	0.829	0.779	0.769	0.790	0.824	0.824	0.885	0.912	0.928	0.940	0.952	0.952	0.938	0.910	0.896
20	1.002	0.843	0.810	0.836	0.905	0.986	1.012	1.039	1.086	1.127	1.134	1.145	1.108	1.074	1.032
25	1.185	1.015	0.914	0.884	0.928	1.035	1.132	1.185	1.228	1.259	1.259	1.264	1.246	1.219	1.153
30	1.356	1.178	0.993	0.958	0.962	1.094	1.234	1.346	1.359	1.382	1.360	1.392	1.376	1.346	1.241
35	1.518	1.295	1.082	1.021	0.998	1.152	1.326	1.472	1.490	1.504	1.487	1.516	1.502	1.479	1.326
40	1.682	1.394	1.196	1.084	1.036	1.208	1.421	1.604	1.635	1.638	1.594	1.621	1.658	1.607	1.405
$\theta = 112\frac{1}{2}^\circ$															
0	0.158	0.158	0.160	0.160	0.167	0.173	0.186	0.191	0.208	0.228	0.251	0.258	0.268	0.275	0.284
1	0.426	0.404	0.398	0.382	0.375	0.387	0.412	0.426	0.431	0.444	0.446	0.458	0.420	0.386	0.362
2	0.512	0.528	0.534	0.542	0.542	0.546	0.542	0.538	0.532	0.532	0.521	0.506	0.502	0.494	0.472
4	0.528	0.544	0.596	0.606	0.629	0.635	0.638	0.642	0.626	0.602	0.588	0.608	0.612	0.606	0.596
6	0.574	0.591	0.631	0.649	0.671	0.678	0.678	0.687	0.679	0.665	0.641	0.653	0.648	0.653	0.642
8	0.615	0.647	0.672	0.695	0.715	0.722	0.726	0.730	0.737	0.723	0.715	0.711	0.718	0.702	0.690
10	0.662	0.689	0.714	0.738	0.756	0.765	0.769	0.772	0.778	0.776	0.772	0.765	0.761	0.758	0.750
15	0.729	0.726	0.742	0.763	0.781	0.829	0.893	0.934	0.956	0.934	0.946	0.963	0.950	0.917	0.906
20	0.796	0.774	0.778	0.786	0.804	0.886	1.000	1.086	1.128	1.179	1.194	1.186	1.125	1.076	1.043
25	0.925	0.878	0.832	0.805	0.830	0.931	1.118	1.239	1.291	1.406	1.390	1.425	1.334	1.259	1.210
30	1.052	0.968	0.894	0.814	0.838	0.968	1.224	1.365	1.469	1.628	1.571	1.630	1.516	1.412	1.348
35	1.196	1.051	0.925	0.782	0.771	0.995	1.312	1.503	1.624	1.843	1.748	1.862	1.725	1.578	1.485
40	1.328	1.142	0.896	0.674	0.726	1.025	1.408	1.611	1.776	2.046	1.896	2.075	1.902	1.726	1.611

TABLE 4 (Continued)

$\frac{r}{R}$	0.237	0.287	0.337	0.387	0.437	0.487	0.537	0.587	0.637	0.687	0.737	0.787	0.837	0.887	0.937
C_J															
$\theta = 135^\circ$															
0	0.158	0.156	0.160	0.160	0.165	0.172	0.178	0.182	0.189	0.204	0.226	0.235	0.243	0.256	0.264
1	0.431	0.425	0.410	0.389	0.377	0.392	0.418	0.426	0.433	0.442	0.428	0.406	0.392	0.364	0.341
2	0.468	0.481	0.495	0.513	0.526	0.528	0.531	0.538	0.546	0.554	0.563	0.561	0.572	0.542	0.522
4	0.502	0.536	0.582	0.608	0.616	0.632	0.638	0.638	0.620	0.594	0.618	0.642	0.628	0.610	0.600
6	0.556	0.574	0.619	0.651	0.658	0.679	0.679	0.685	0.674	0.661	0.667	0.686	0.673	0.657	0.642
8	0.602	0.632	0.654	0.690	0.706	0.718	0.718	0.733	0.729	0.725	0.715	0.722	0.716	0.702	0.688
10	0.658	0.674	0.692	0.724	0.745	0.754	0.762	0.773	0.778	0.786	0.772	0.768	0.757	0.750	0.739
15	0.693	0.719	0.738	0.758	0.806	0.869	0.899	0.949	0.992	1.024	0.990	0.962	0.912	0.892	0.872
20	0.736	0.748	0.771	0.789	0.822	0.958	1.024	1.102	1.188	1.224	1.228	1.154	1.088	1.026	1.004
25	0.745	0.752	0.749	0.675	0.709	0.906	1.115	1.237	1.345	1.448	1.452	1.378	1.269	1.221	1.181
30	0.723	0.691	0.563	0.498	0.587	0.842	1.098	1.358	1.516	1.638	1.656	1.582	1.452	1.398	1.326
35	0.696	0.478	0.380	0.385	0.482	0.789	1.087	1.506	1.678	1.836	1.861	1.790	1.644	1.574	1.478
40	0.662	0.326	0.215	0.286	0.400	0.728	1.094	1.612	1.805	2.021	2.048	1.074	1.829	1.743	1.611
$\theta = 167\frac{1}{2}^\circ$															
0	0.162	0.162	0.162	0.165	0.169	0.175	0.178	0.186	0.194	0.208	0.216	0.234	0.242	0.249	0.266
1	0.426	0.413	0.400	0.386	0.374	0.392	0.416	0.430	0.441	0.438	0.432	0.418	0.389	0.352	0.314
2	0.474	0.486	0.492	0.498	0.510	0.526	0.534	0.554	0.558	0.560	0.554	0.559	0.563	0.555	0.543
4	0.486	0.514	0.544	0.572	0.603	0.621	0.626	0.628	0.635	0.633	0.644	0.661	0.642	0.625	0.608
6	0.532	0.556	0.598	0.634	0.645	0.678	0.687	0.687	0.697	0.692	0.705	0.693	0.681	0.662	0.645
8	0.589	0.598	0.624	0.668	0.683	0.714	0.742	0.742	0.735	0.744	0.767	0.745	0.725	0.709	0.681
10	0.642	0.646	0.675	0.692	0.729	0.762	0.783	0.803	0.814	0.809	0.803	0.788	0.768	0.754	0.732
15	0.699	0.708	0.728	0.765	0.817	0.914	0.968	1.002	1.035	1.054	1.002	0.984	0.943	0.925	0.857
20	0.748	0.761	0.784	0.804	0.911	1.032	1.102	1.189	1.218	1.234	1.209	1.176	1.112	1.072	1.000
25	0.622	0.560	0.527	0.697	0.835	1.058	1.159	1.314	1.421	1.473	1.438	1.429	1.376	1.264	1.172
30	0.439	0.328	0.263	0.478	0.693	0.957	1.203	1.426	1.597	1.658	1.641	1.630	1.598	1.425	1.314
35	0.316	0.156	0.094	0.255	0.552	0.832	1.180	1.538	1.779	1.829	1.860	1.841	1.762	1.571	1.430
40	0.108	-0.174	-0.165	-0.004	0.386	0.716	1.146	1.624	1.952	2.043	2.058	2.013	1.916	1.684	1.506
$\theta = 180^\circ$															
0	0.162	0.162	0.160	0.164	0.168	0.172	0.178	0.186	0.191	0.200	0.208	0.214	0.229	0.238	0.246
1	0.416	0.404	0.386	0.378	0.388	0.402	0.428	0.446	0.456	0.448	0.436	0.418	0.392	0.350	0.308
2	0.486	0.495	0.509	0.521	0.540	0.558	0.562	0.560	0.565	0.572	0.578	0.572	0.564	0.558	0.531
4	0.486	0.506	0.541	0.578	0.621	0.635	0.640	0.642	0.646	0.648	0.650	0.658	0.640	0.628	0.604
6	0.532	0.548	0.586	0.614	0.654	0.681	0.695	0.698	0.703	0.705	0.711	0.697	0.675	0.662	0.638
8	0.576	0.591	0.623	0.652	0.689	0.718	0.732	0.759	0.768	0.763	0.758	0.732	0.728	0.710	0.677
10	0.631	0.642	0.658	0.681	0.712	0.756	0.778	0.805	0.812	0.810	0.802	0.786	0.761	0.745	0.709
15	0.693	0.716	0.735	0.758	0.865	0.928	0.964	1.027	1.045	1.045	1.024	0.973	0.938	0.880	0.832
20	0.728	0.742	0.769	0.782	0.958	1.052	1.132	1.218	1.248	1.236	1.201	1.146	1.086	1.012	0.965
25	0.589	0.593	0.573	0.625	0.794	1.038	1.249	1.385	1.459	1.474	1.460	1.395	1.341	1.215	1.142
30	0.336	0.271	0.276	0.396	0.623	0.987	1.356	1.536	1.672	1.685	1.685	1.667	1.552	1.396	1.285
35	0.193	0.094	0.112	0.183	0.458	0.942	1.448	1.703	1.856	1.916	1.823	1.830	1.774	1.575	1.427
40	-0.042	-0.210	-0.161	-0.022	0.326	0.914	1.537	1.842	2.034	2.128	2.136	2.181	1.982	1.748	1.542

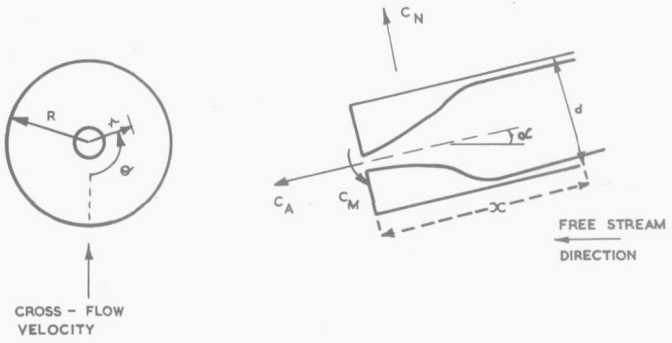

FIG. 1. DEFINITION OF SYMBOLS.

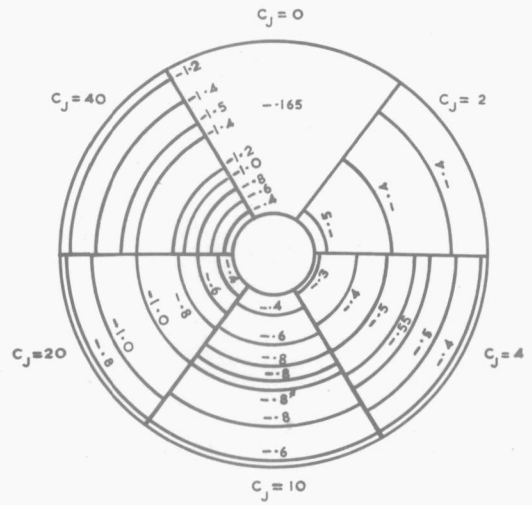

FIG. 2a. PRESSURE DISTRIBUTION ON BASE AT ZERO INCIDENCE.

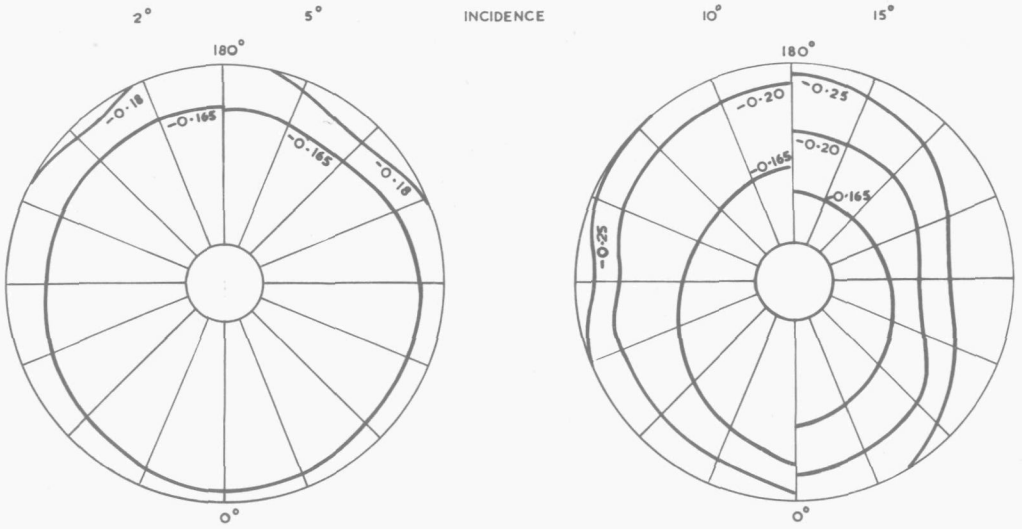

FIG 2b. BLUFF AFTER BODY. BASE PRESSURE DISTRIBUTION $C_J=0$

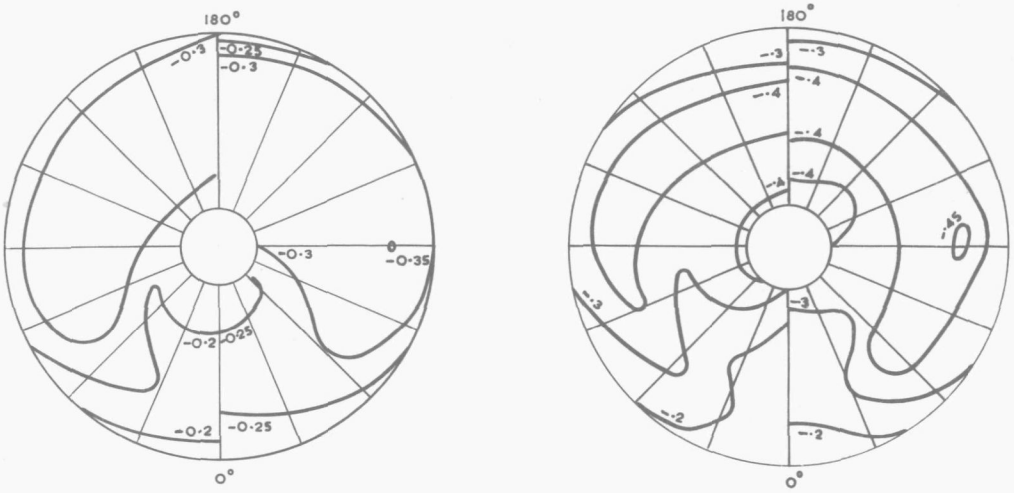

FIG. 2c. BASE PRESSURE DISTRIBUTION $C_J=1$

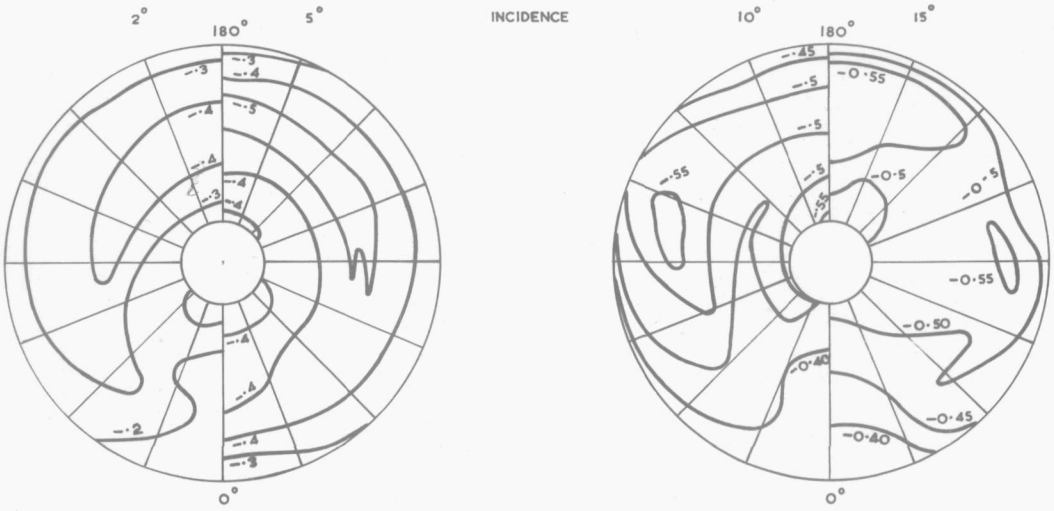

FIG. 2d. BASE PRESSURE DISTRIBUTION $C_J = 2$

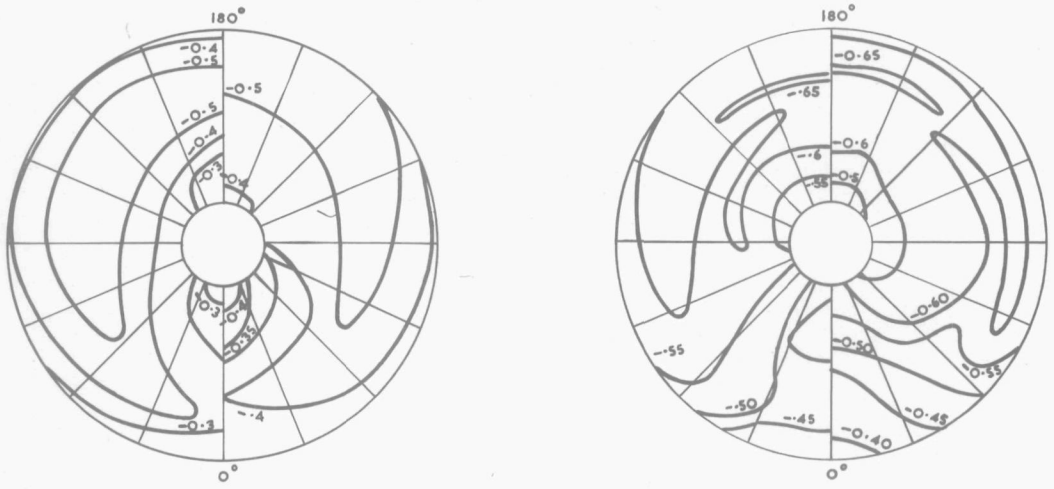

FIG. 2e. BASE PRESSURE DISTRIBUTION $C_J = 4$

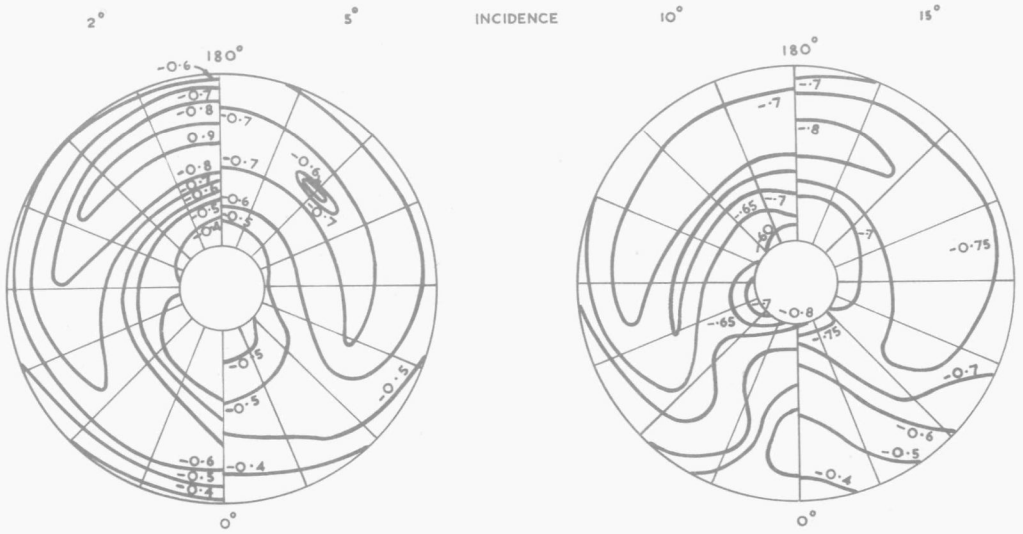

FIG. 2f. BASE PRESSURE DISTRIBUTION $C_J = 10$

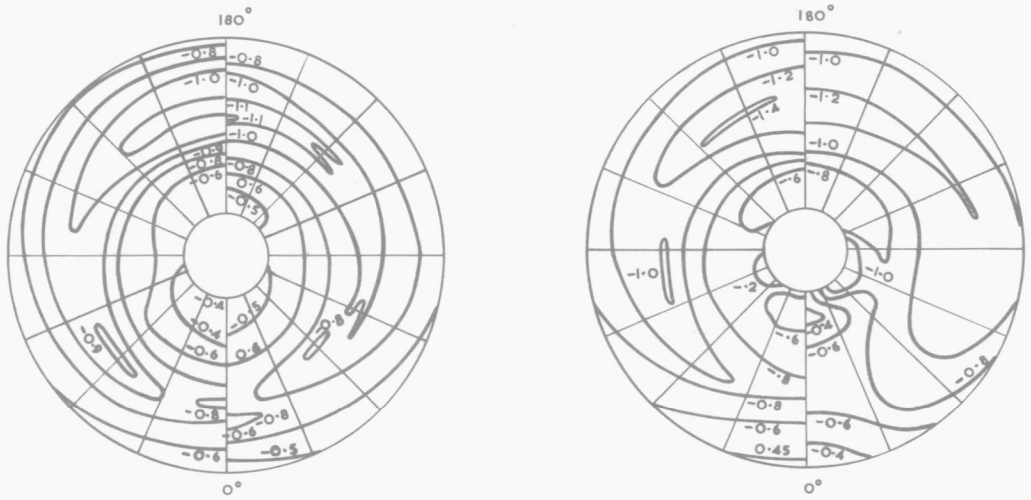

FIG. 2g. BASE PRESSURE DISTRIBUTION $C_J = 20$

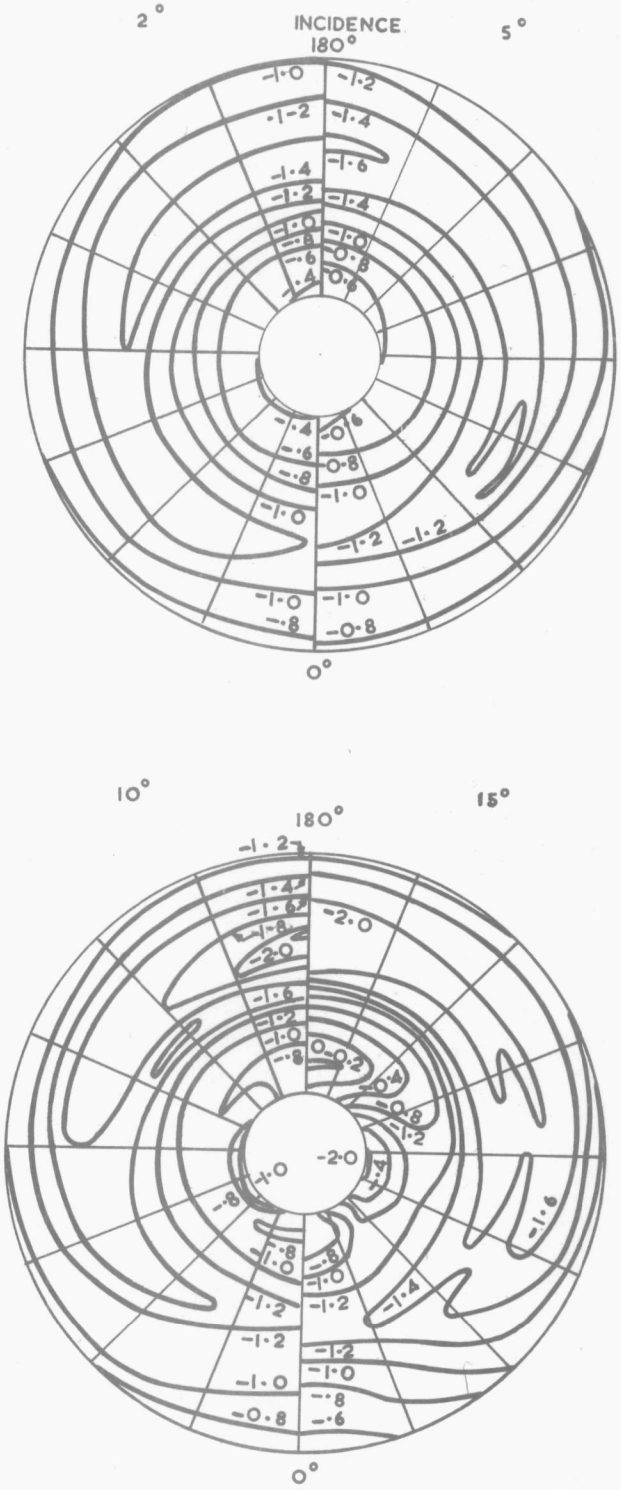

FIG. 2h. BASE PRESSURE DISTRIBUTION $C_J = 40$

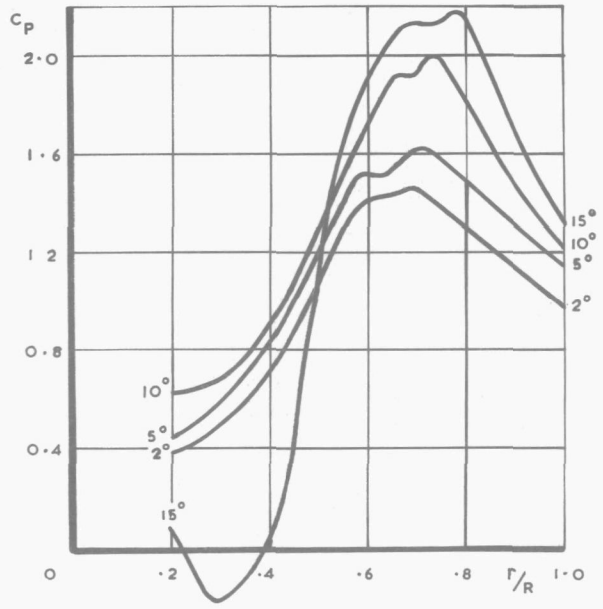

FIG. 3. TYPICAL VARIATION OF RADIAL PRESSURE DISTRIBUTION ON THE BASE WITH INCIDENCE C_J=40 Θ=180°

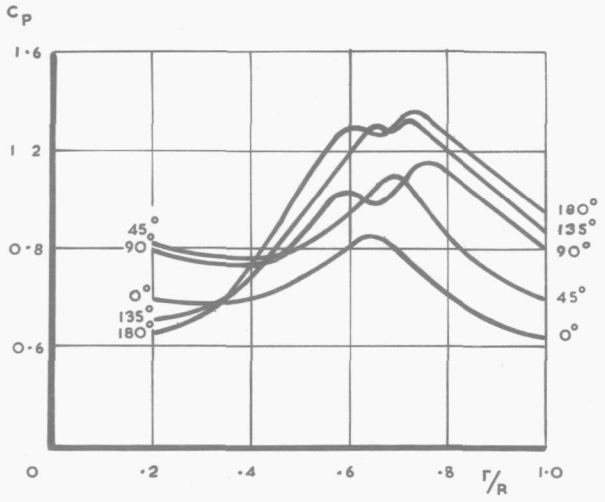

FIG. 4. TYPICAL VARIATION OF RADIAL PRESSURE DISTRIBUTION ON BASE WITH MERIDIAN ANGLE C_J= 20 α=10°

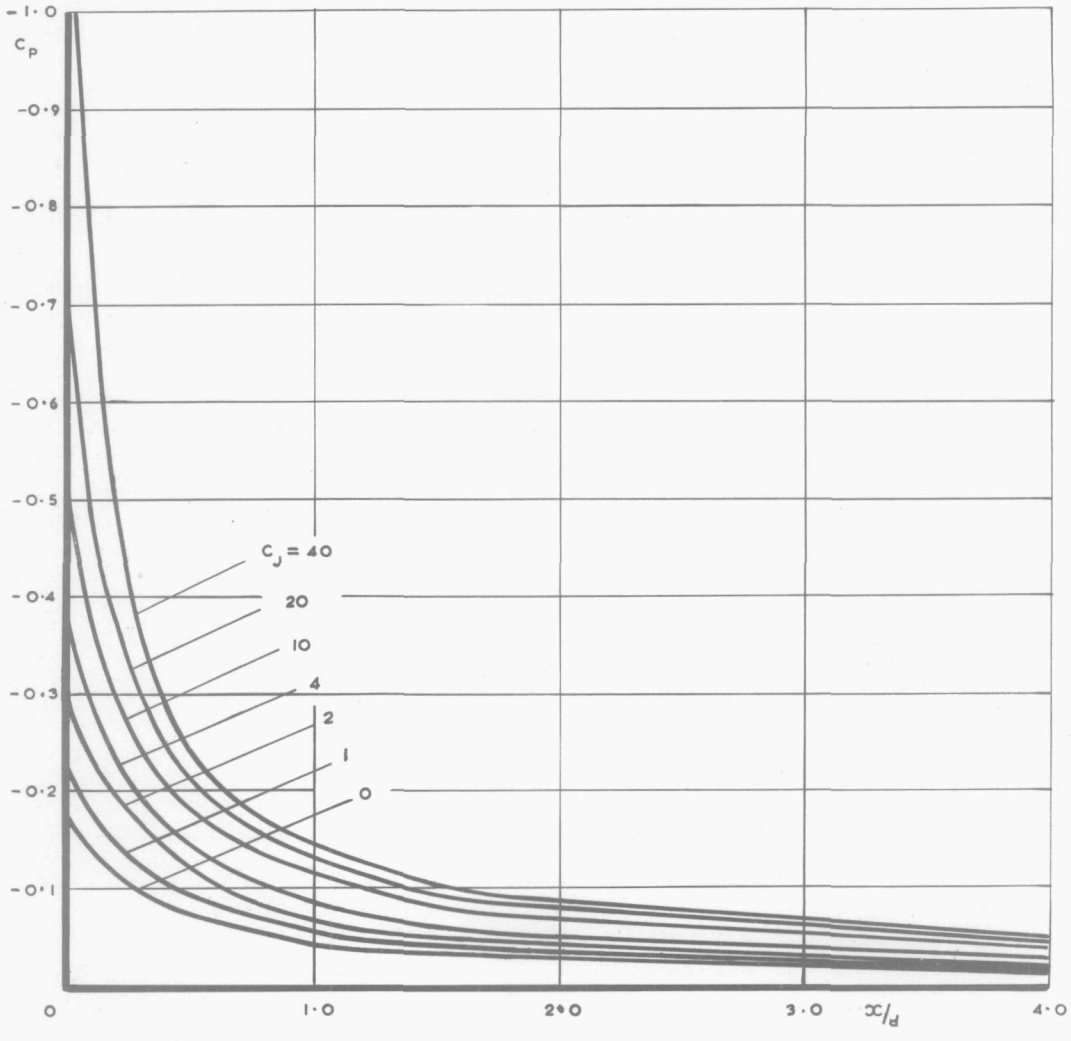

FIG. 5a. BLUFF AFTERBODY - SIDE PRESSURE DISTRIBUTION-ZERO INCIDENCE

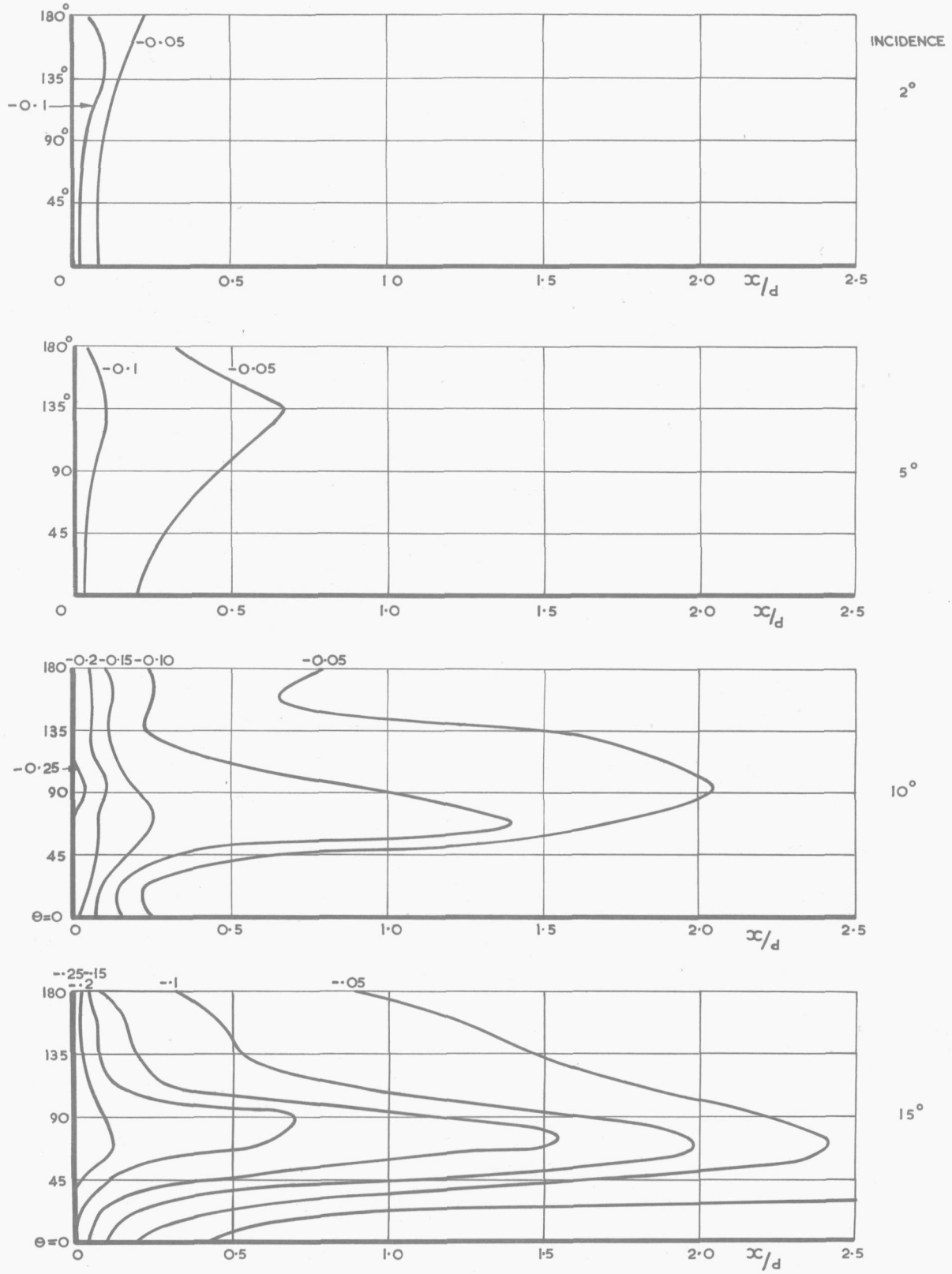

FIG. 5b. BLUFF AFTERBODY – SIDE PRESSURE DISTRIBUTION $C_J = 0$

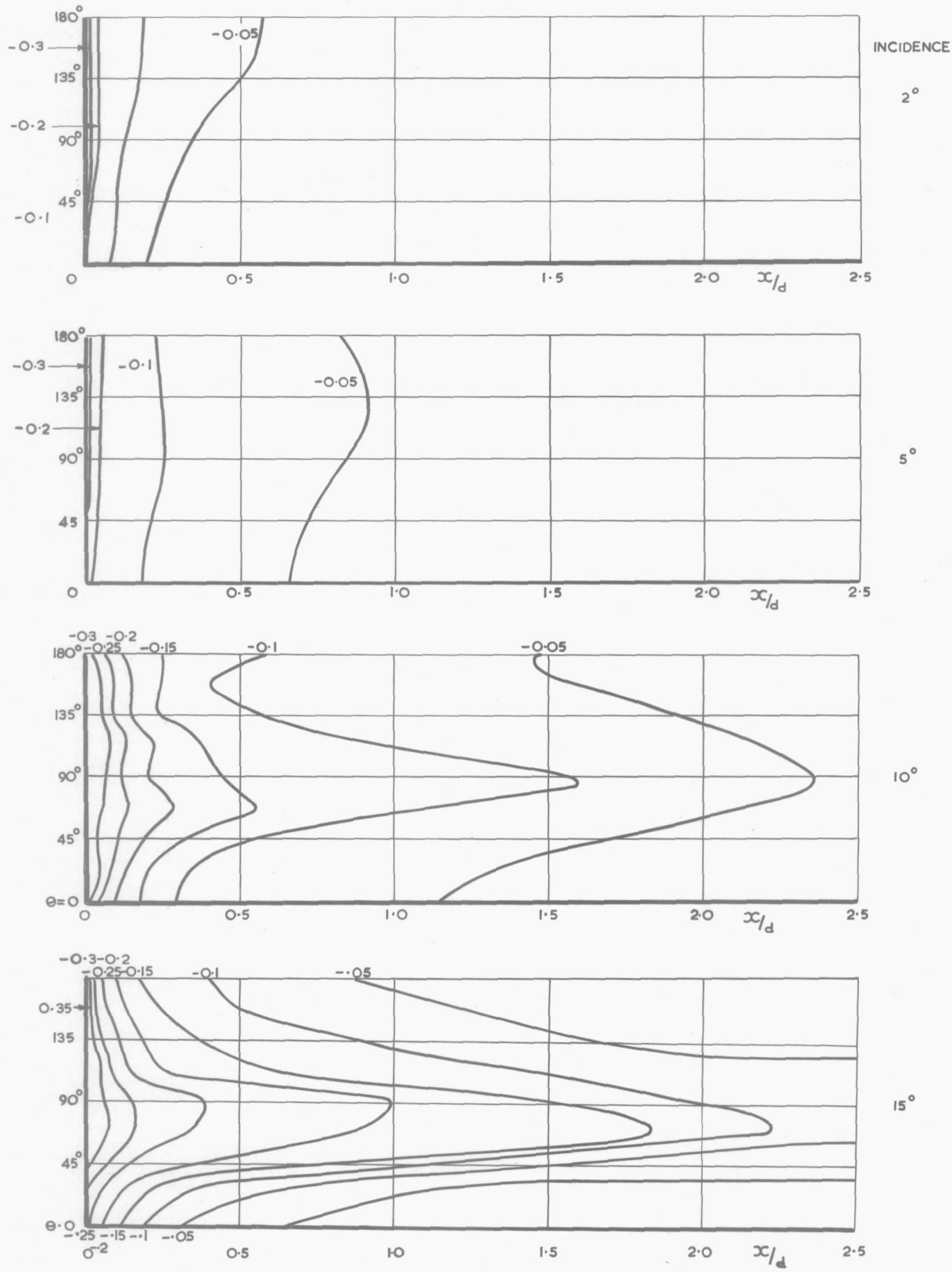

FIG. 5c. BLUFF AFTERBODY - SIDE PRESSURE DISTRIBUTION $C_J = 1$

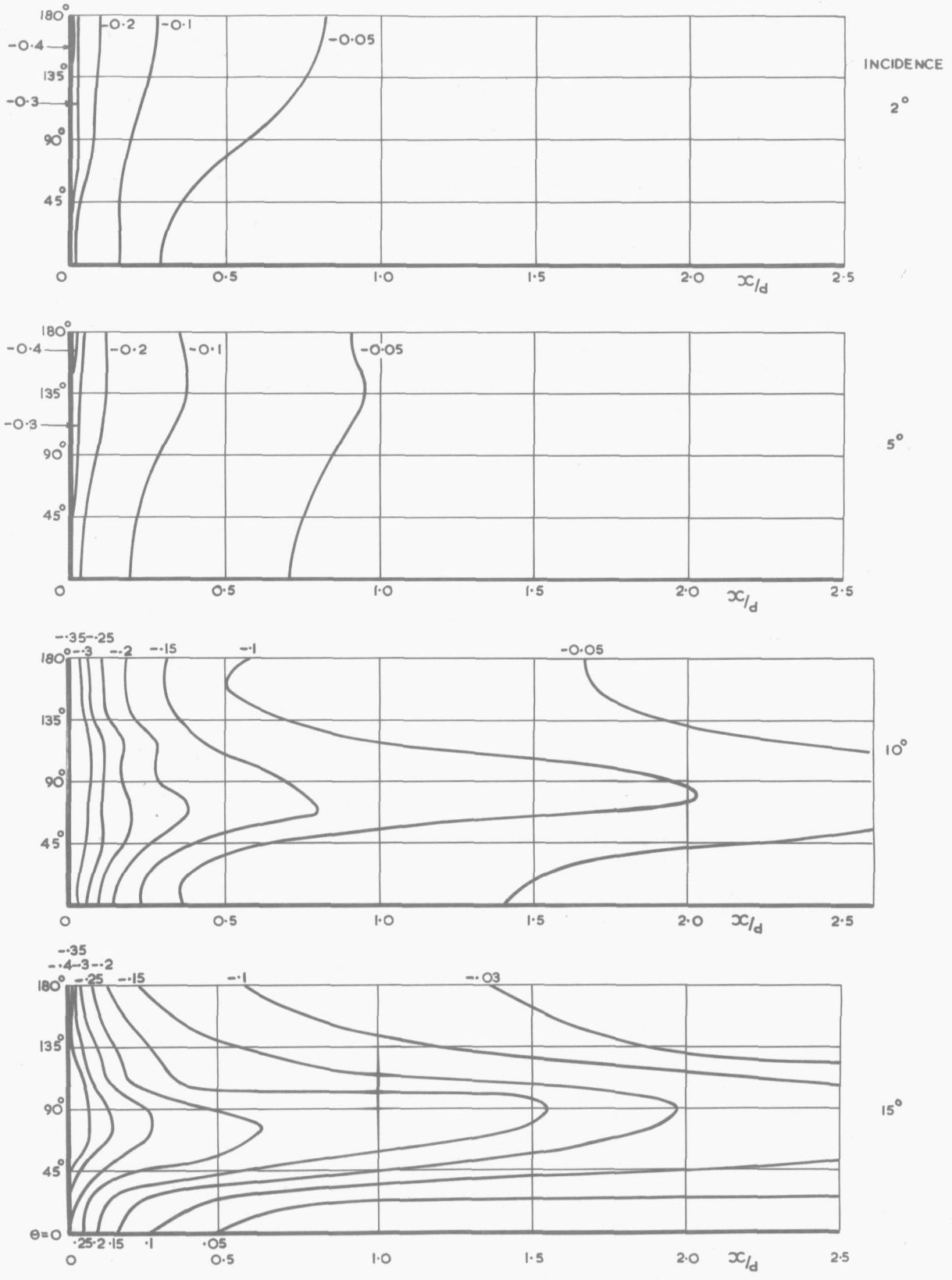

FIG. 5d. BLUFF AFTERBODY - SIDE PRESSURE DISTRIBUTION $C_J = 2$

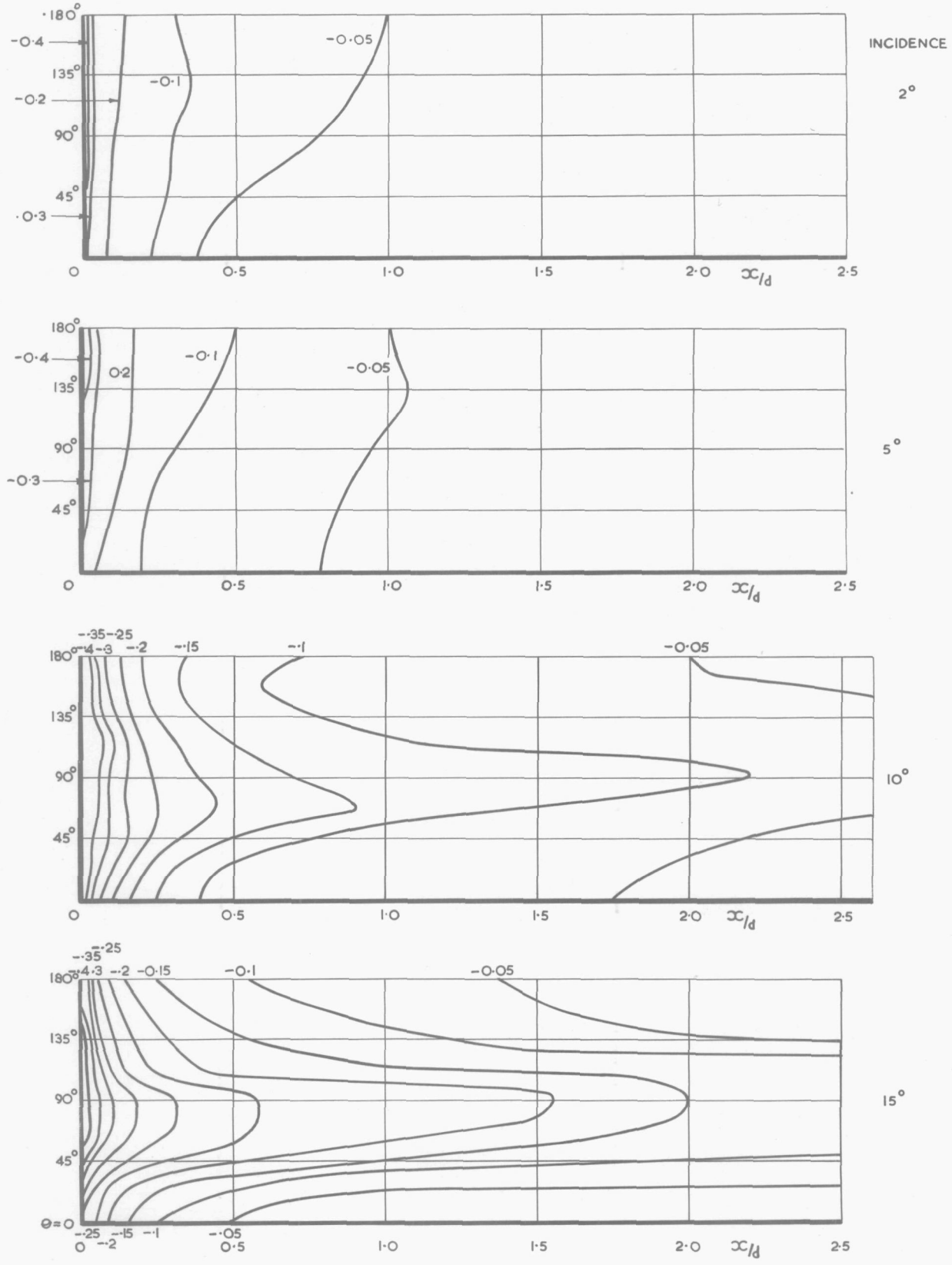

FIG. 5e. BLUFF AFTERBODY - SIDE PRESSURE DISTRIBUTION $C_J = 4$

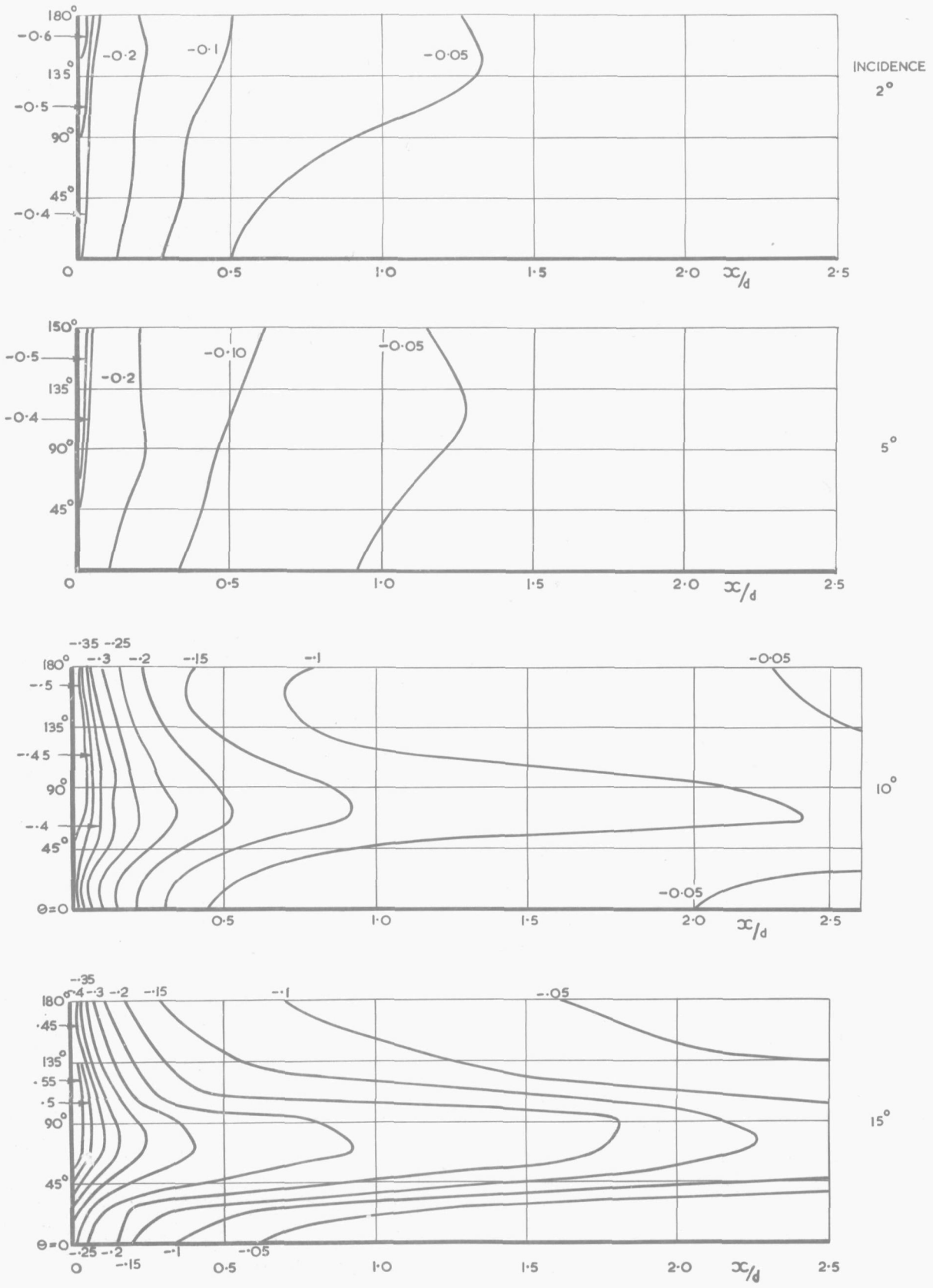

FIG. 5f. BLUFF AFTERBODY - SIDE PRESSURE DISTRIBUTION $C_J = 10$

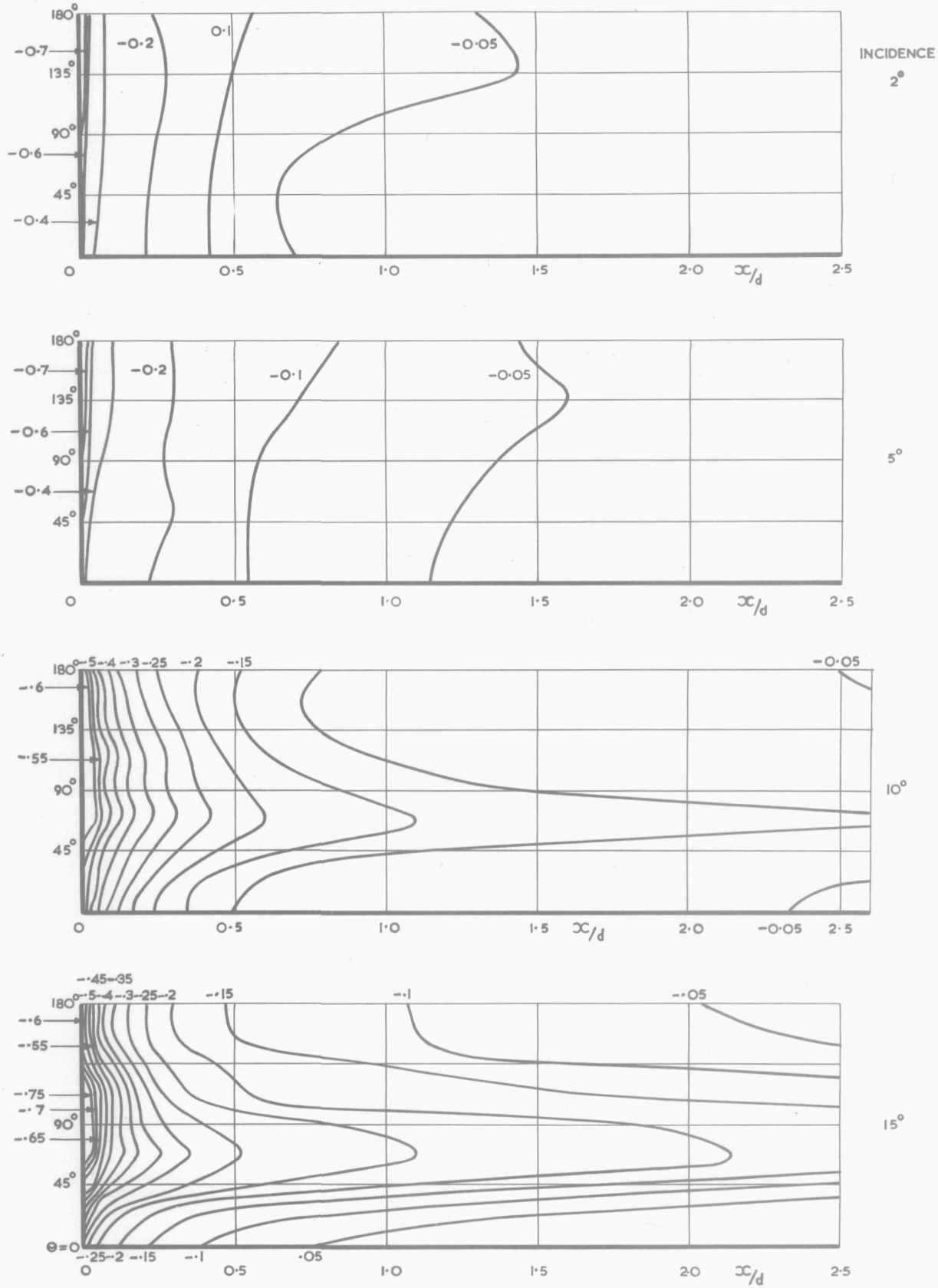

FIG. 5g. BLUFF AFTERBODY - SIDE PRESSURE DISTRIBUTION C_J=20

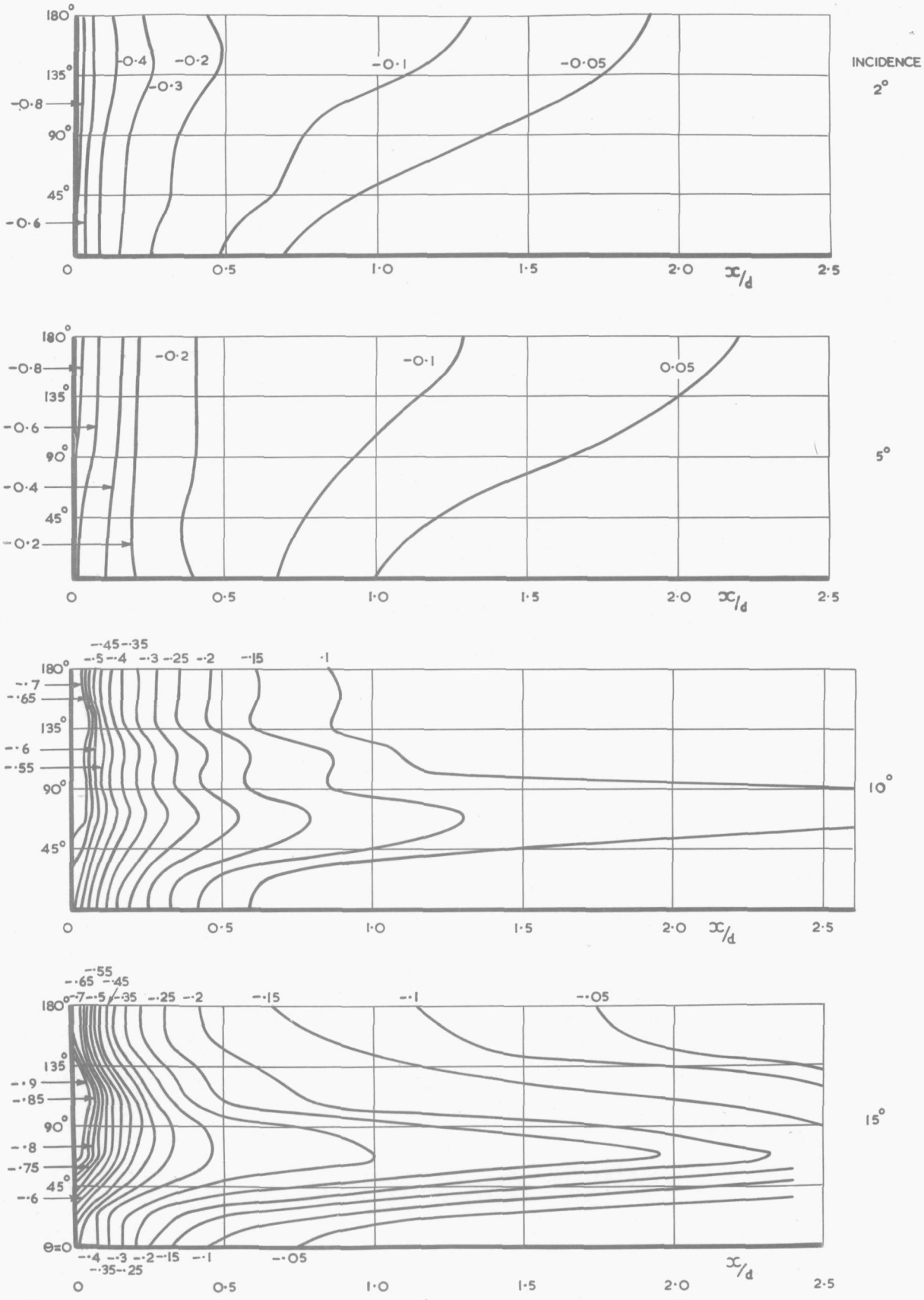

FIG. 5h. BLUFF AFTERBODY SIDE PRESSURE DISTRIBUTION C_J=40

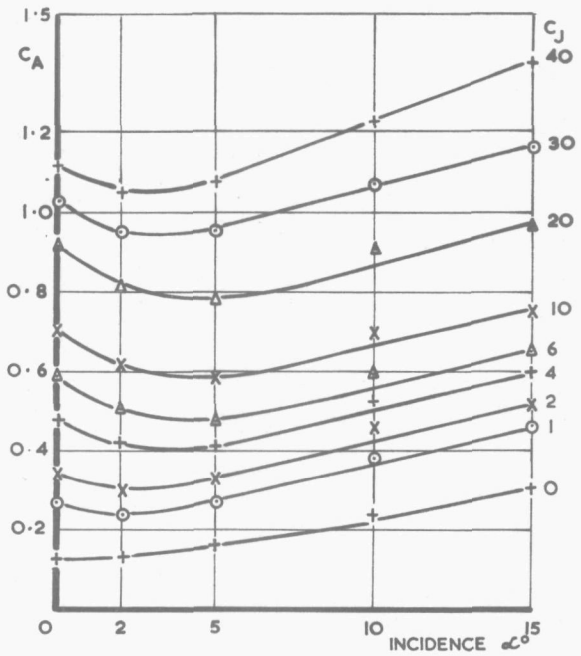

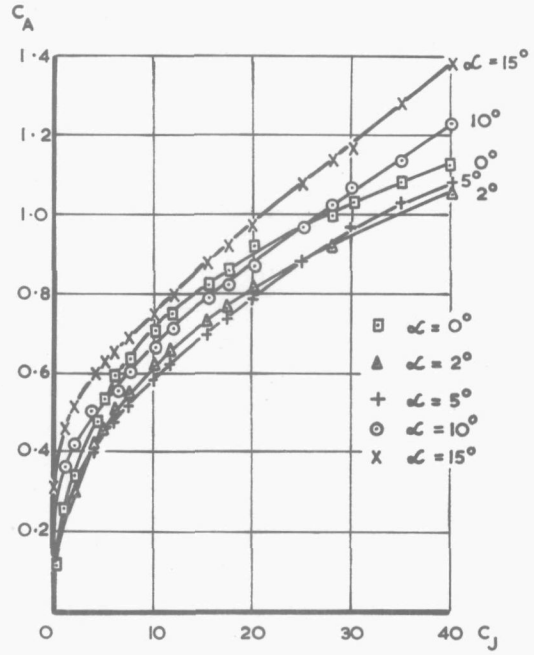

FIG. 6. BLUFF AFTERBODY - VARIATION OF AXIAL FORCE COEFFICIENT WITH INCIDENCE α & C_J

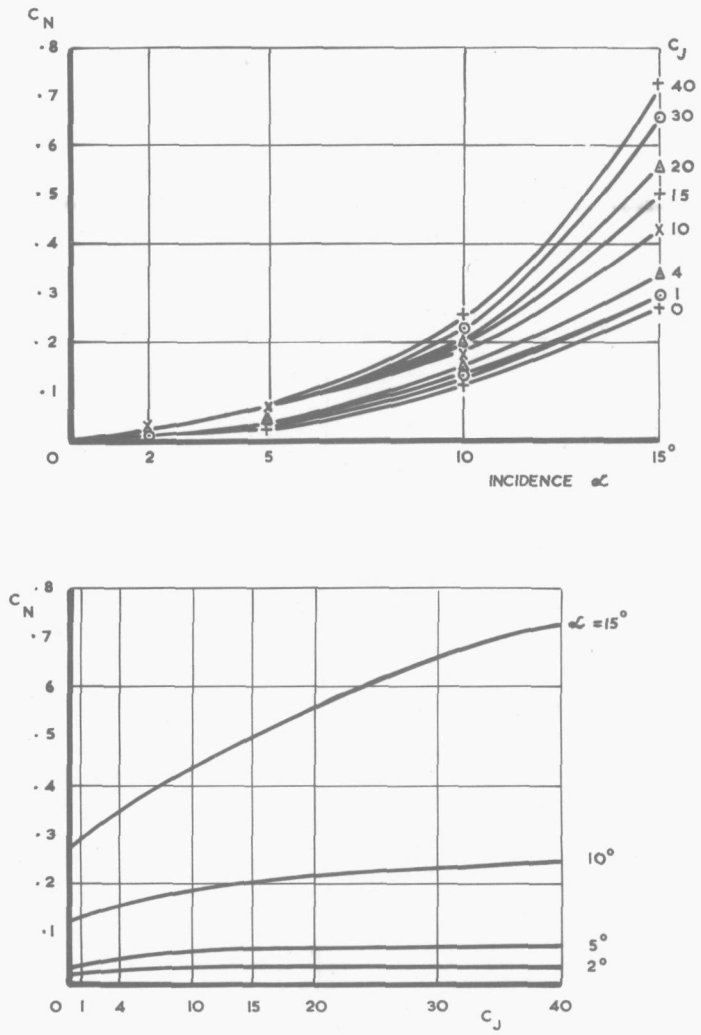

FIG. 7. BLUFF AFTERBODY – VARIATION OF NORMAL FORCE COEFFICIENT WITH INCIDENCE ∝ & C_J

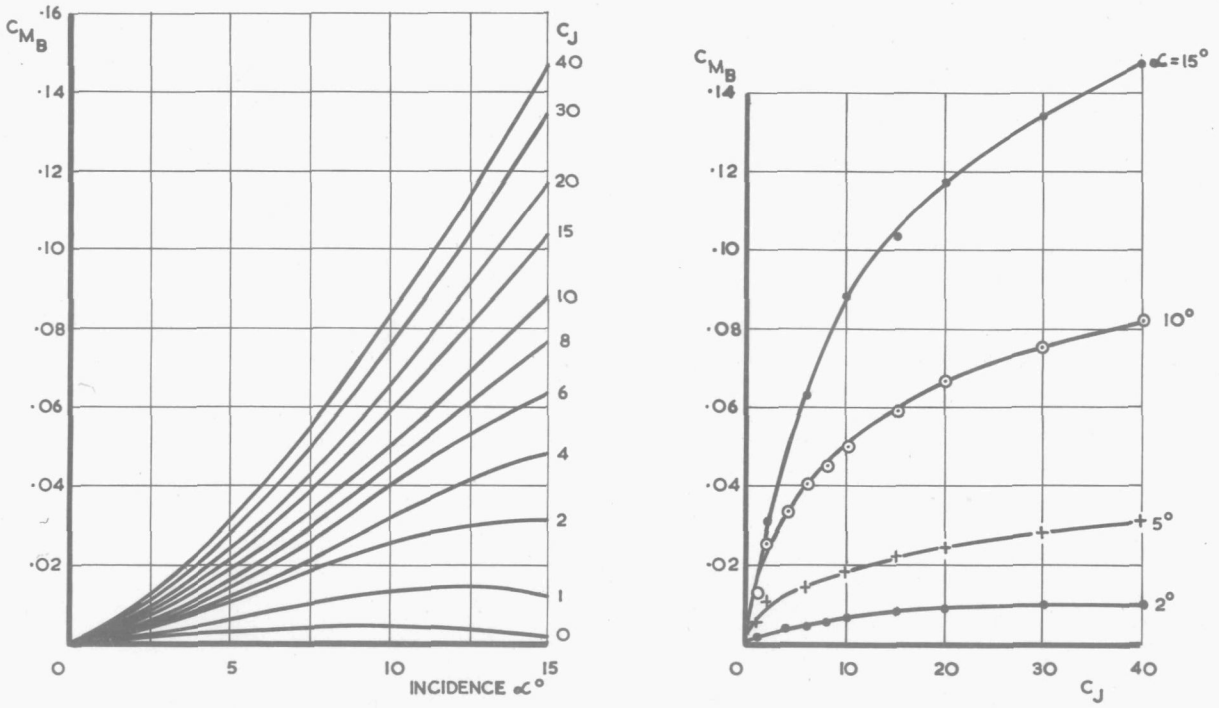

FIG. 8. BLUFF AFTERBODY-VARIATION OF PITCHING MOMENT DUE TO BASE PRESSURES.

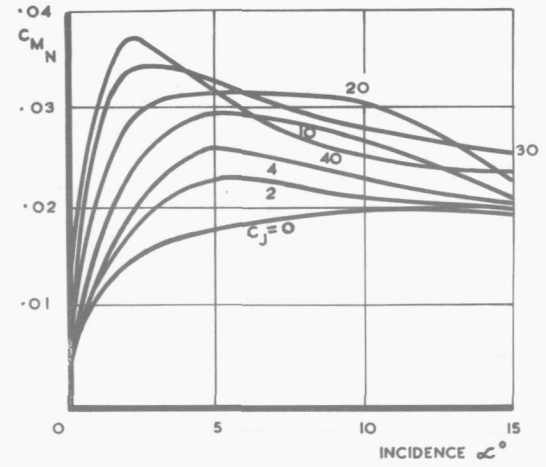

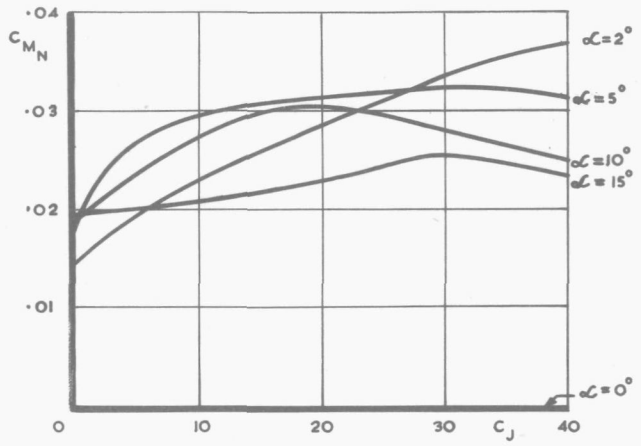

FIG. 9. BLUFF AFTERBODY – VARIATION OF PITCHING MOMENT DUE TO SIDE PRESSURES

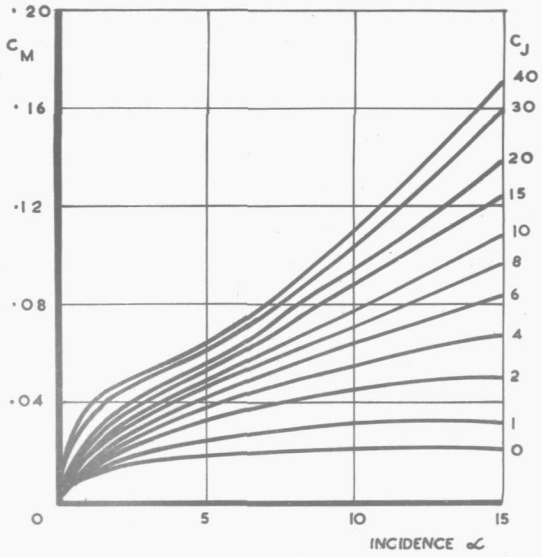

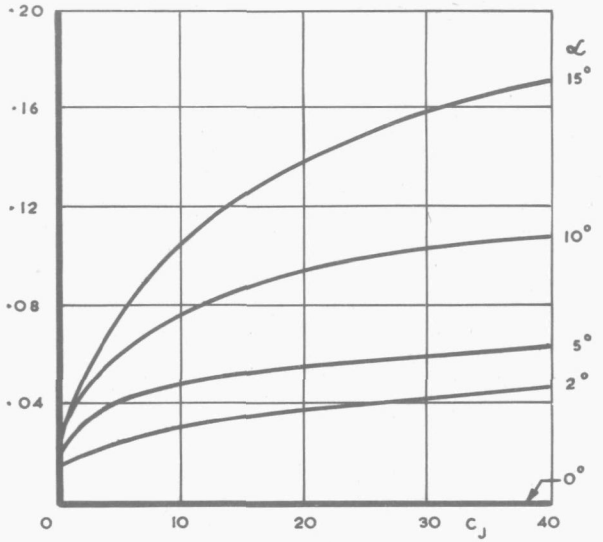

FIG. 10. BLUFF AFTERBODY – VARIATION OF TOTAL PITCHING MOMENT WITH INCIDENCE & C_J

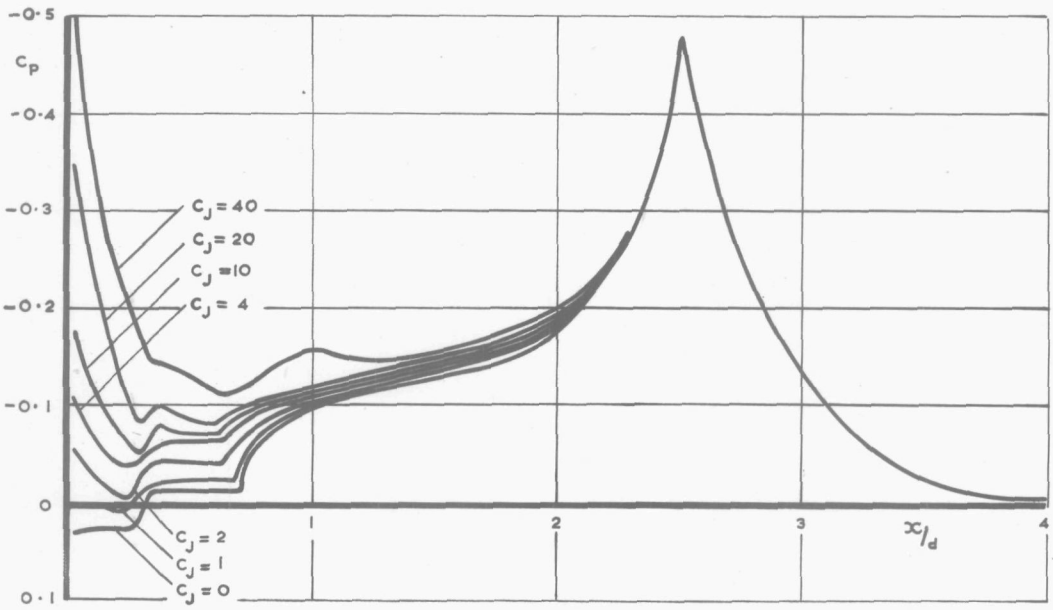

FIG. 11a. PRESSURE DISTRIBUTION ON CONICAL AFTERBODY-ZERO INCIDENCE

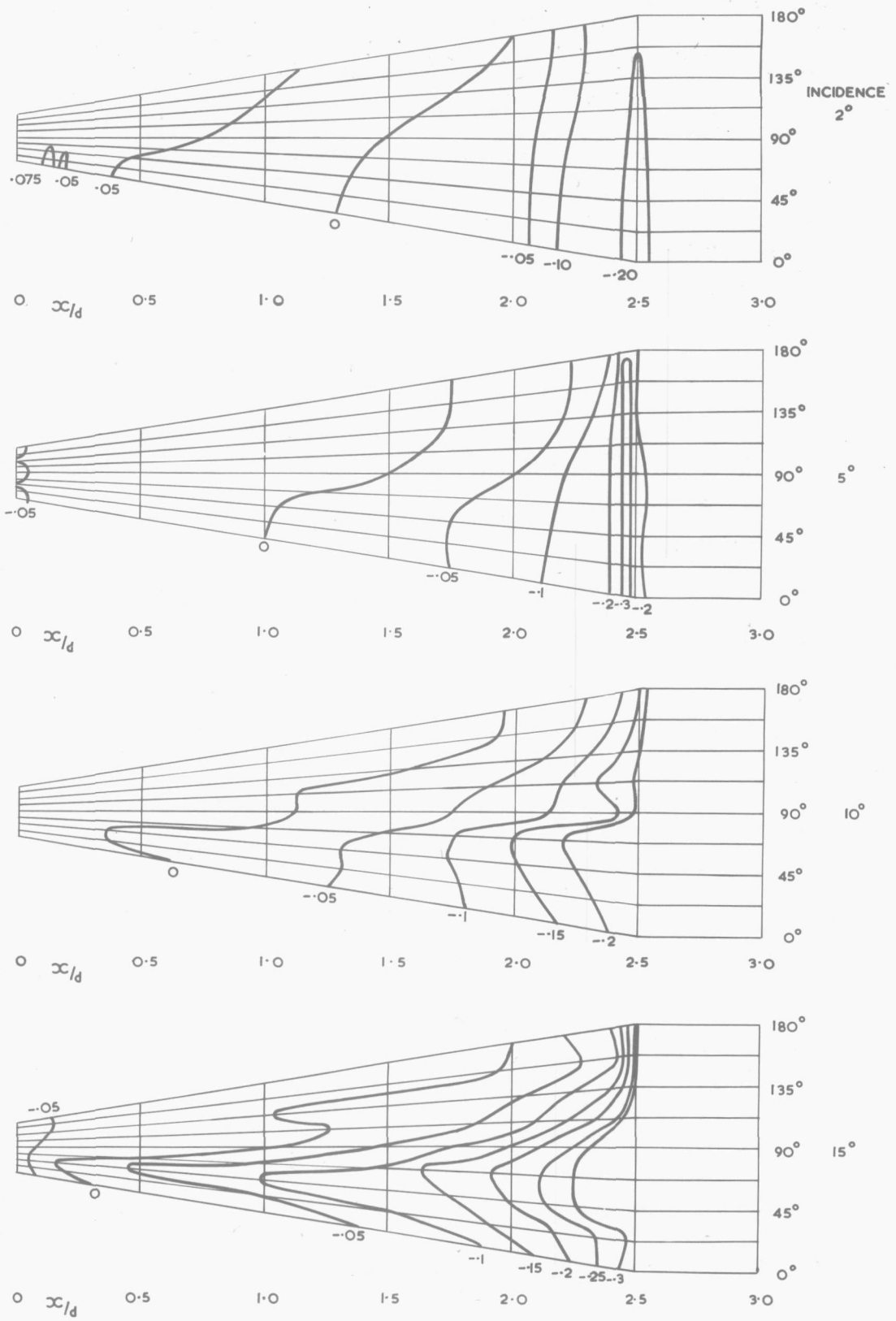

FIG. 11b. CONICAL AFTERBODY PRESSURE DISTRIBUTION $C_J = 0$

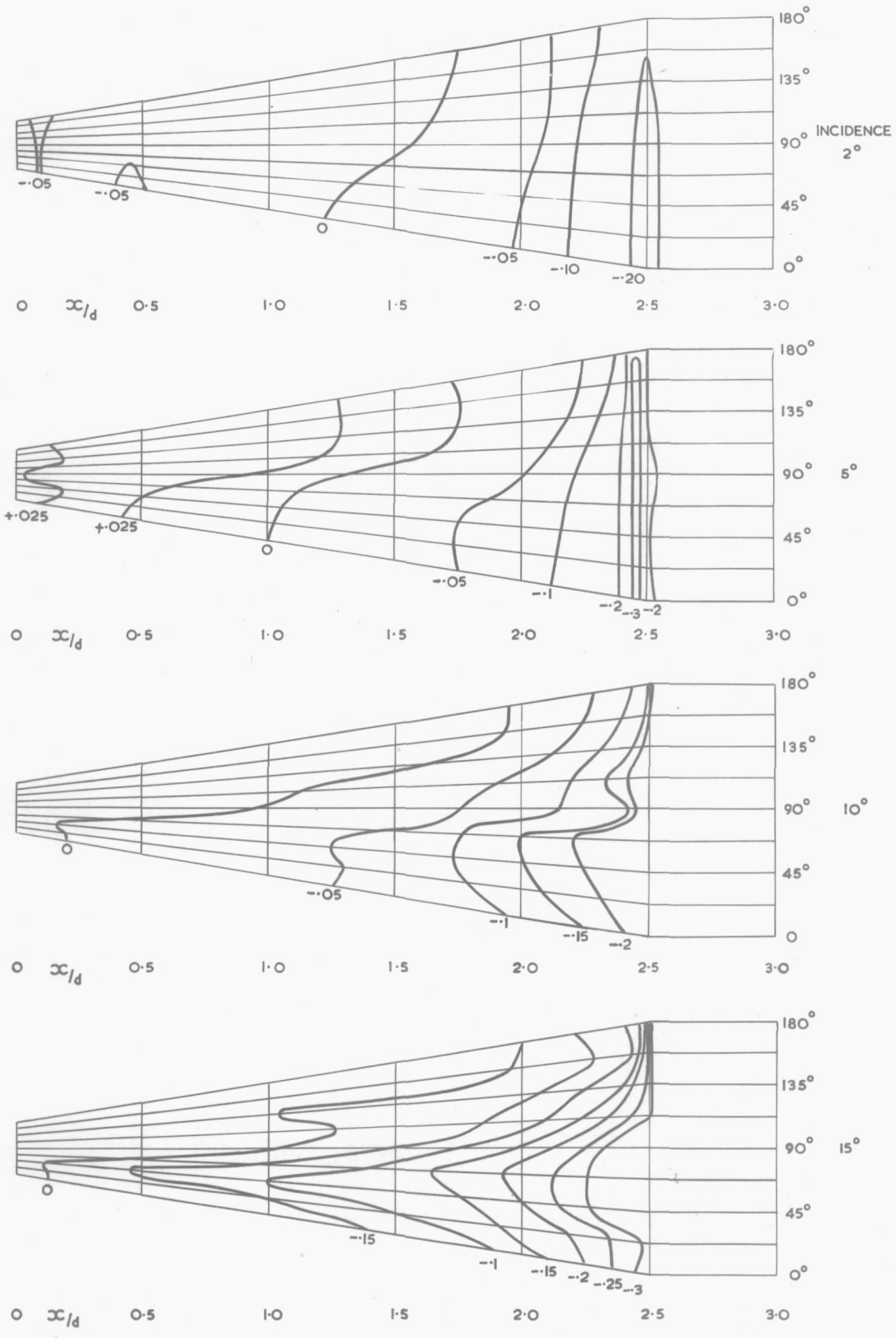

FIG. 11c. CONICAL AFTERBODY PRESSURE DISTRIBUTION $C_J = 1$

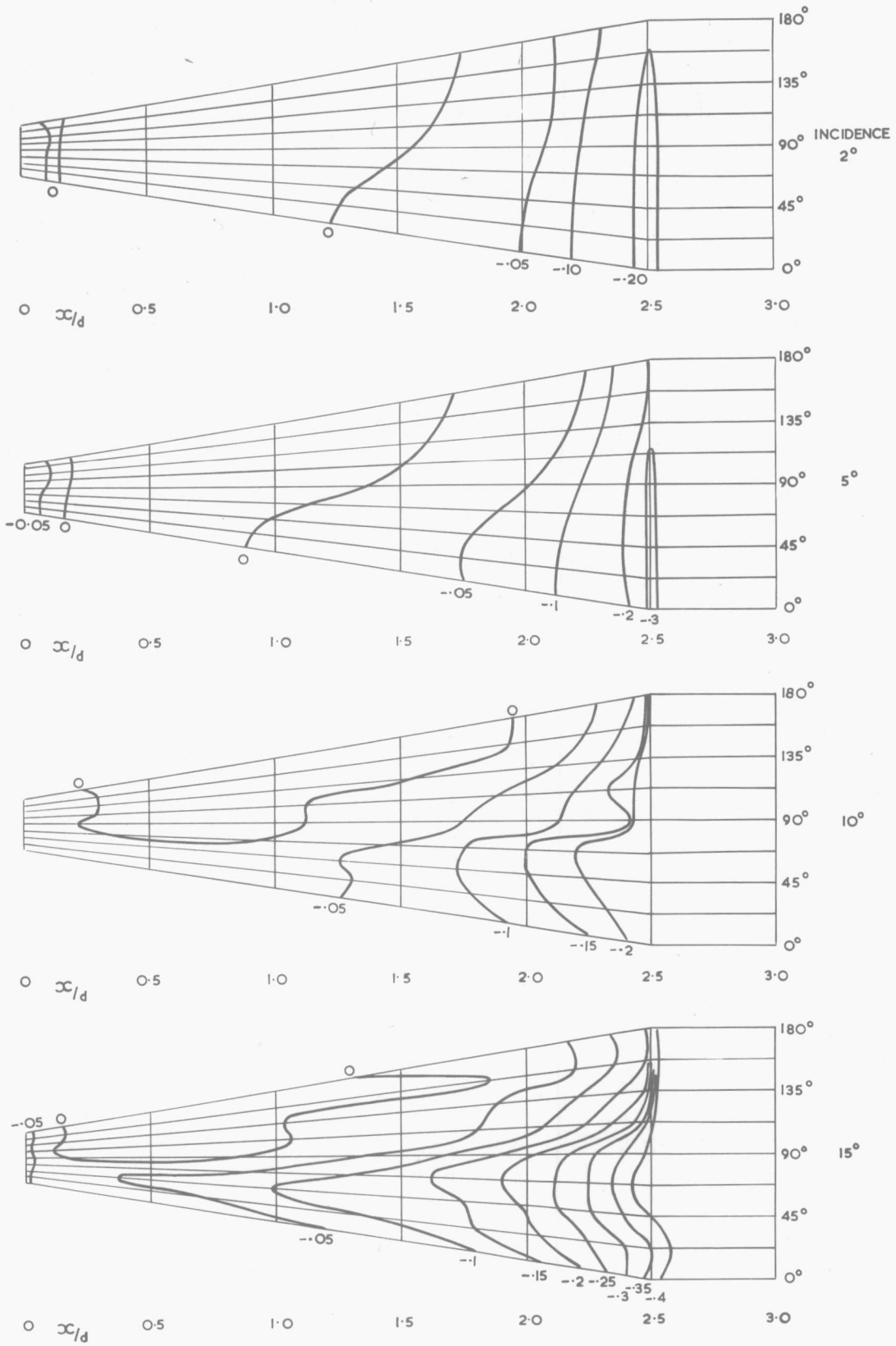

FIG. 11d. CONICAL AFTERBODY PRESSURE DISTRIBUTION $C_J = 2$

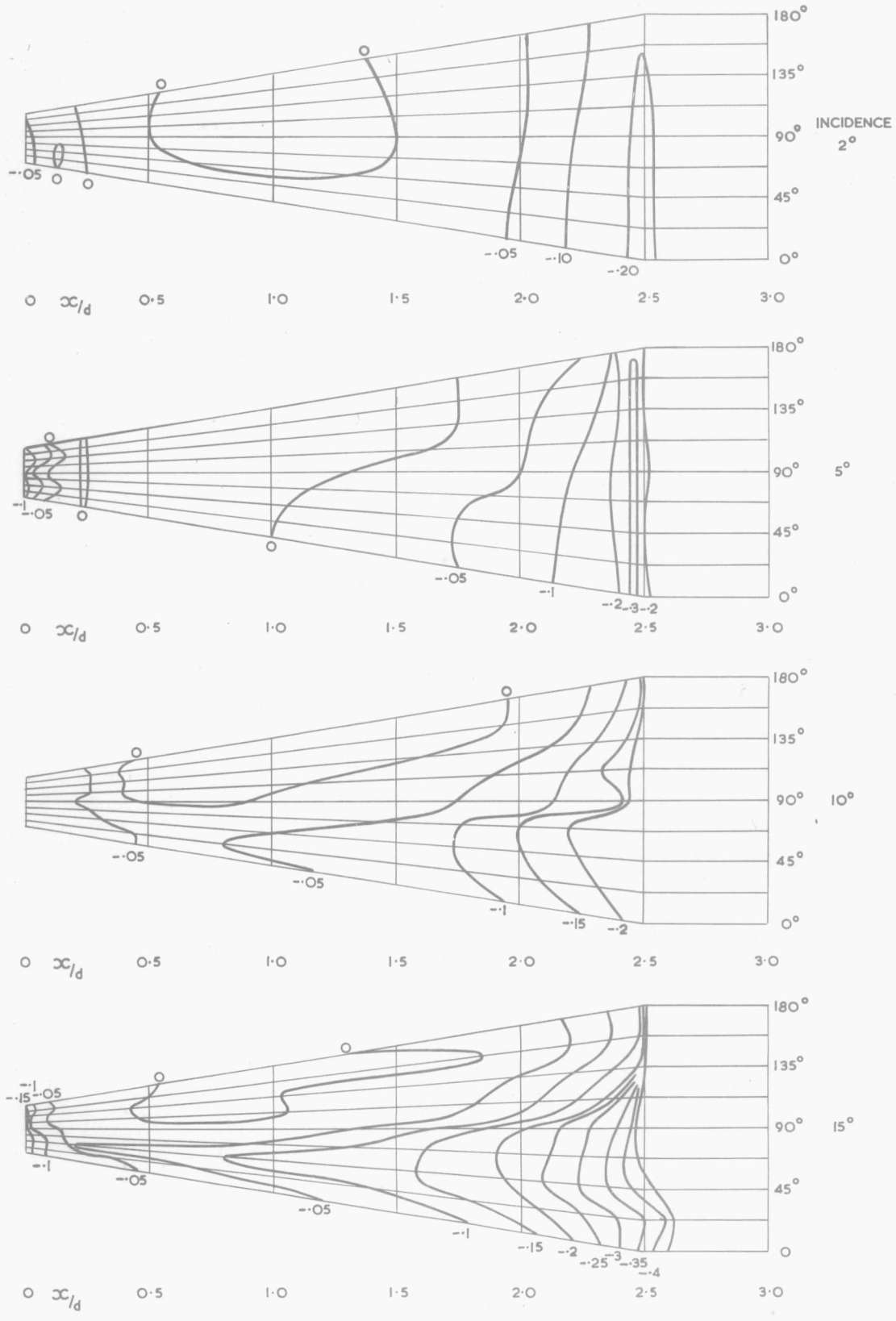

FIG 11e. CONICAL AFTERBODY PRESSURE DISTRIBUTION $C_J=4$

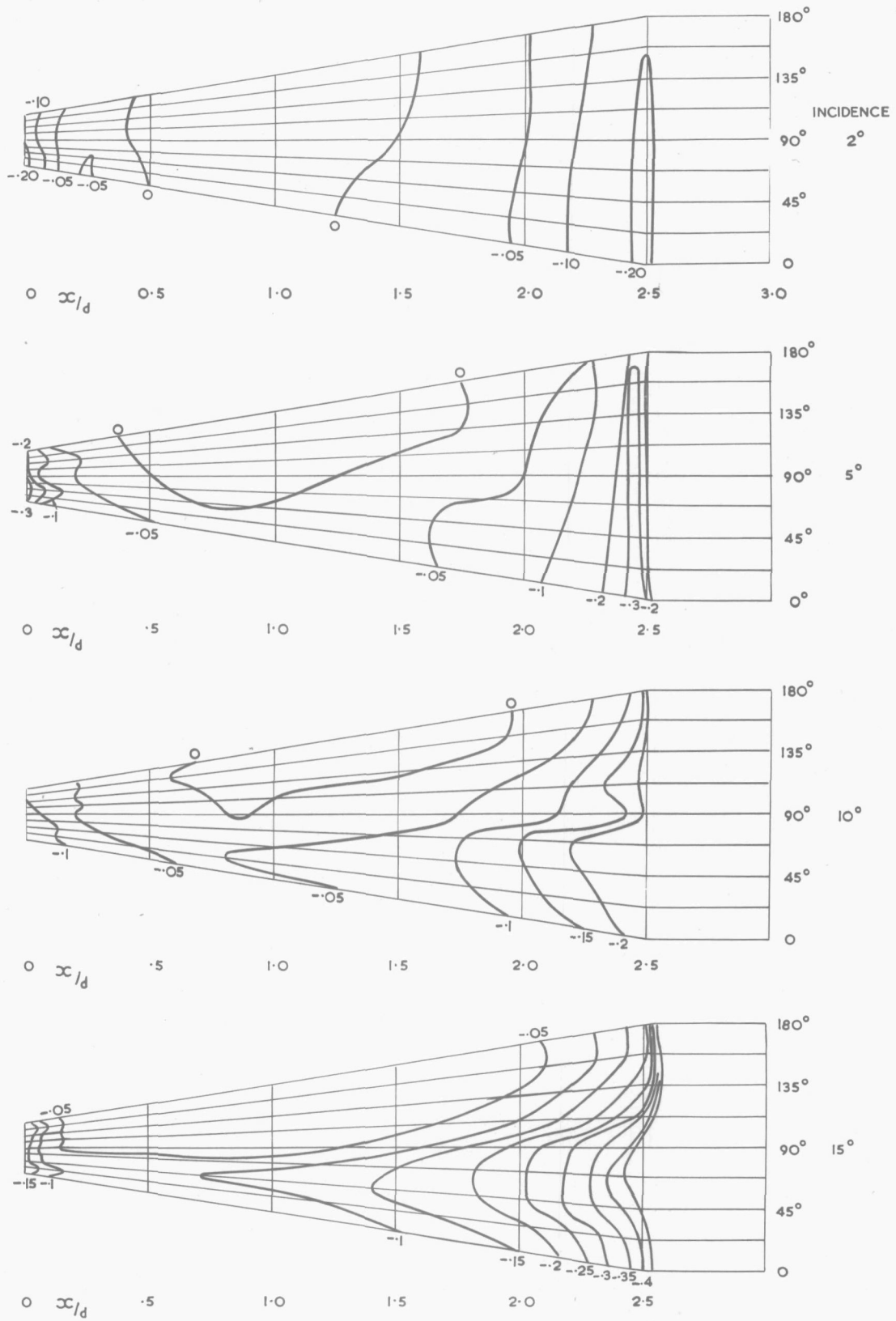

FIG. 11f. CONICAL AFTERBODY PRESSURE DISTRIBUTION $C_J = 10$

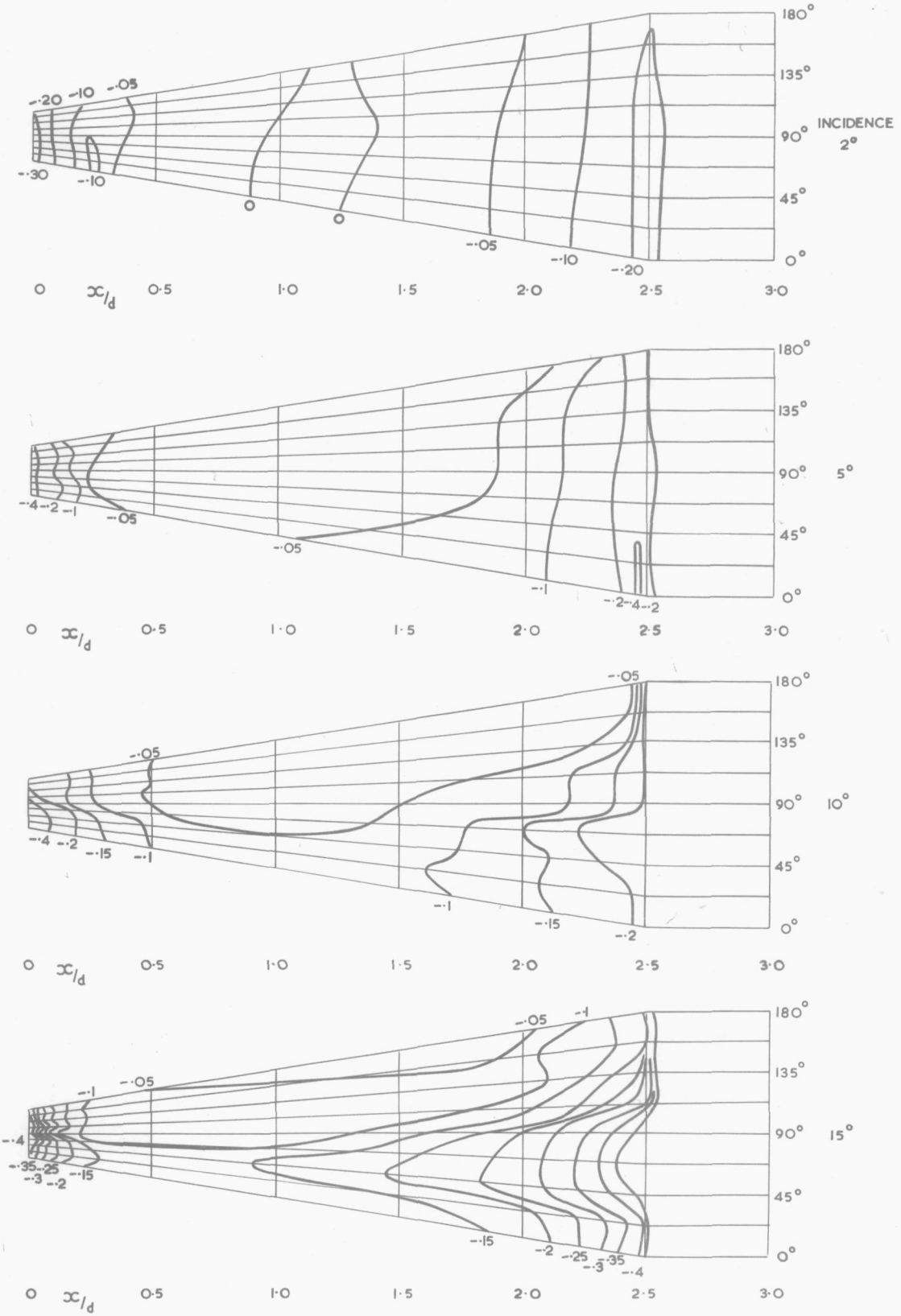

FIG. 11g. CONICAL AFTERBODY PRESSURE DISTRIBUTION $C_J = 20$

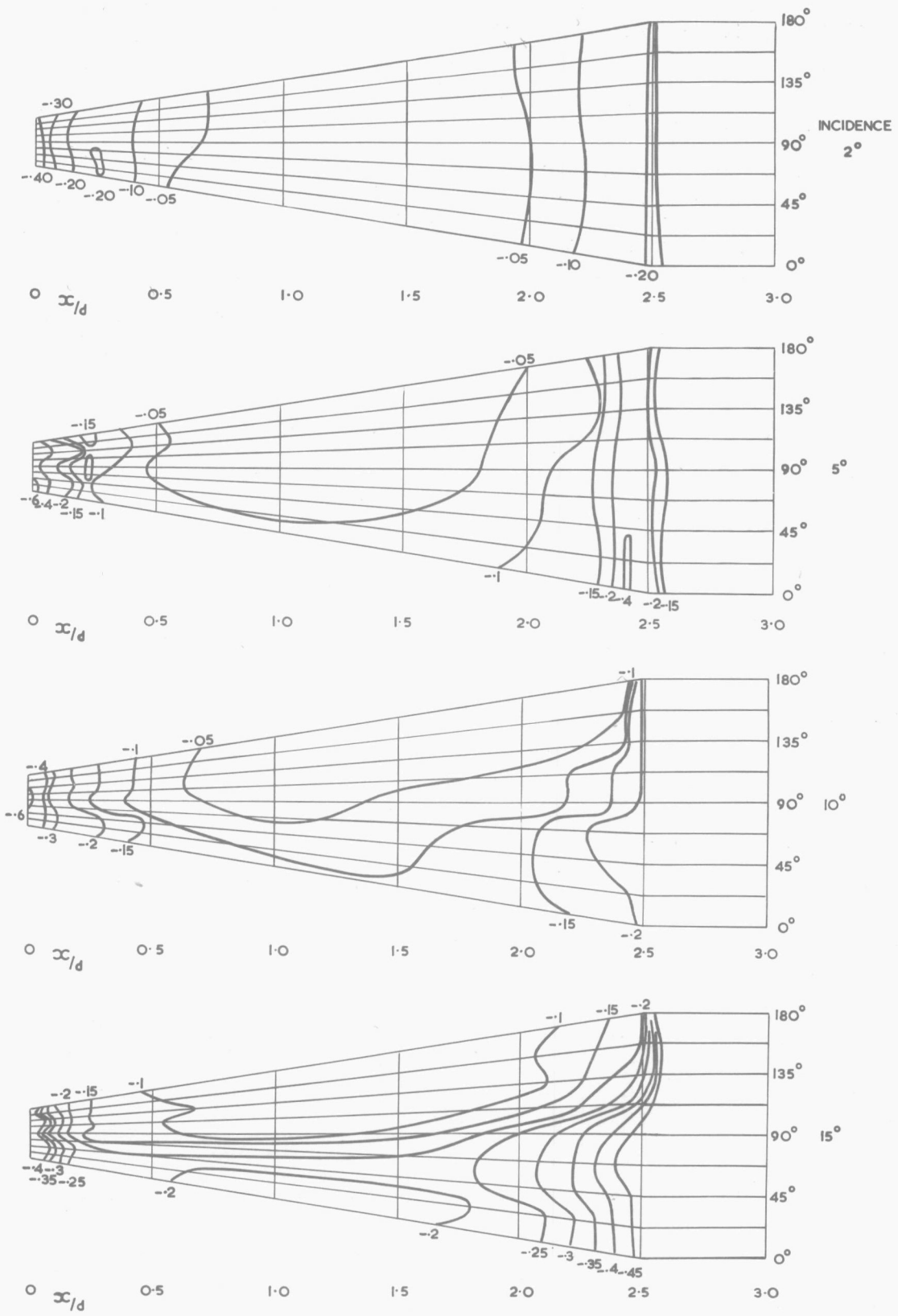

FIG. 11h. CONICAL AFTERBODY PRESSURE DISTRIBUTION $C_J = 40$

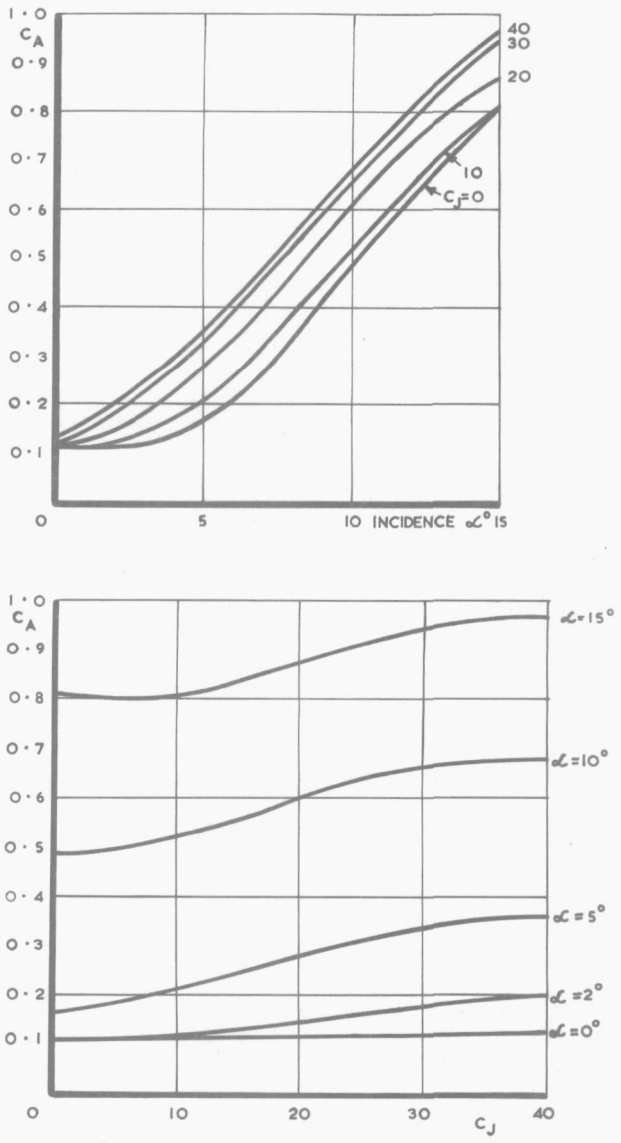

FIG. 12. CONICAL AFTERBODY — VARIATION OF AXIAL FORCE COEFFICIENT WITH INCIDENCE & C_J

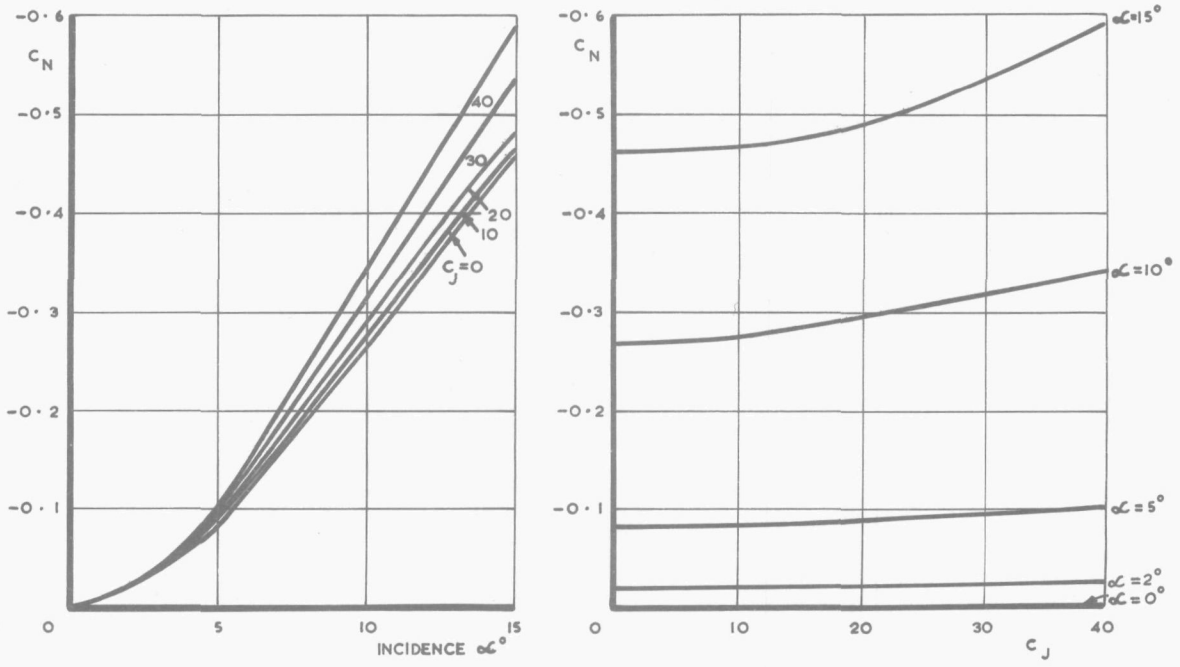

FIG. 13. CONICAL AFTERBODY - VARIATION OF NORMAL FORCE COEFFICIENT WITH INCIDENCE & C_J

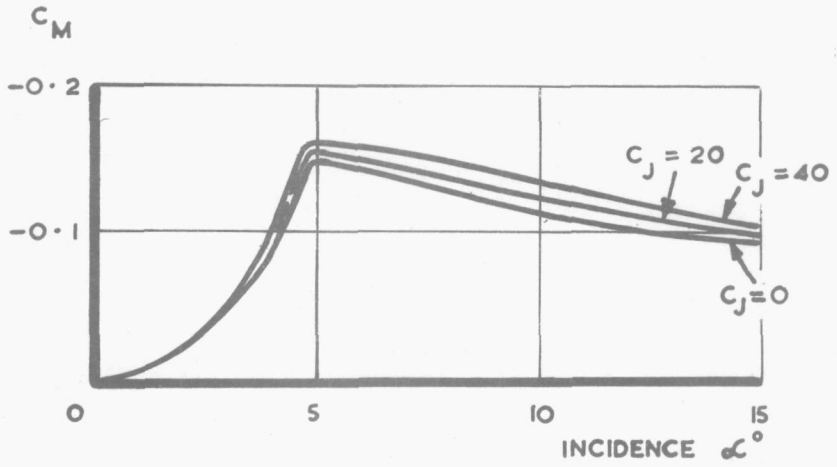

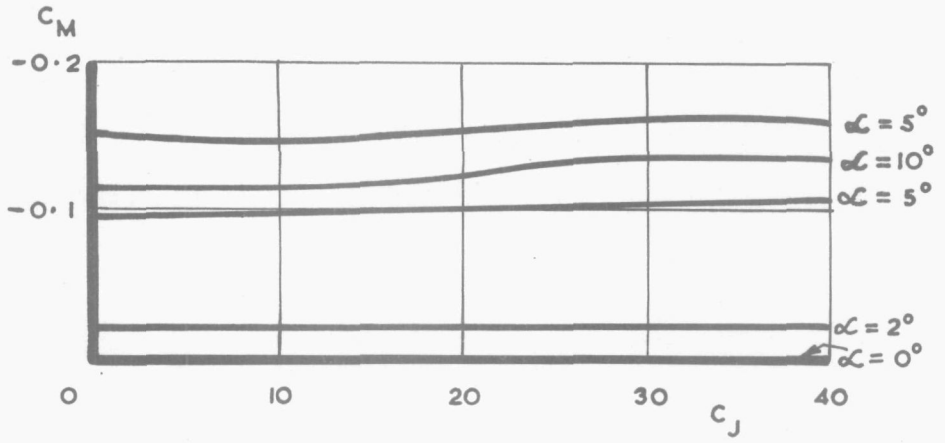

FIG. 14. CONICAL AFTERBODY - VARIATION OF PITCHING MOMENT COEFFICIENT WITH INCIDENCE & C_J

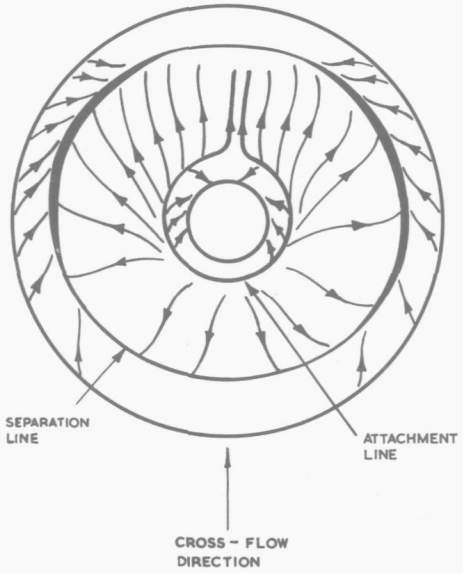

FIG. 15. BASE FLOW DETAILS

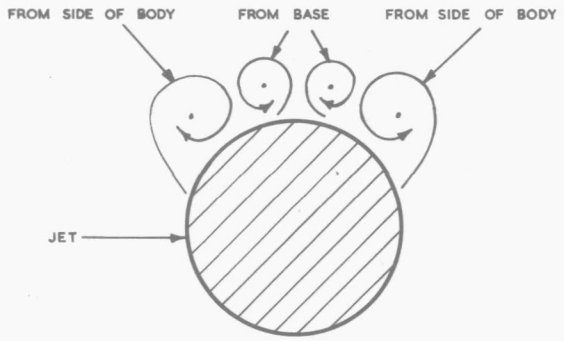

FIG. 16 a. RELATIVE POSITIONS OF THE JET & VORTICES DOWNSTREAM OF THE BASE NOT TO SCALE.

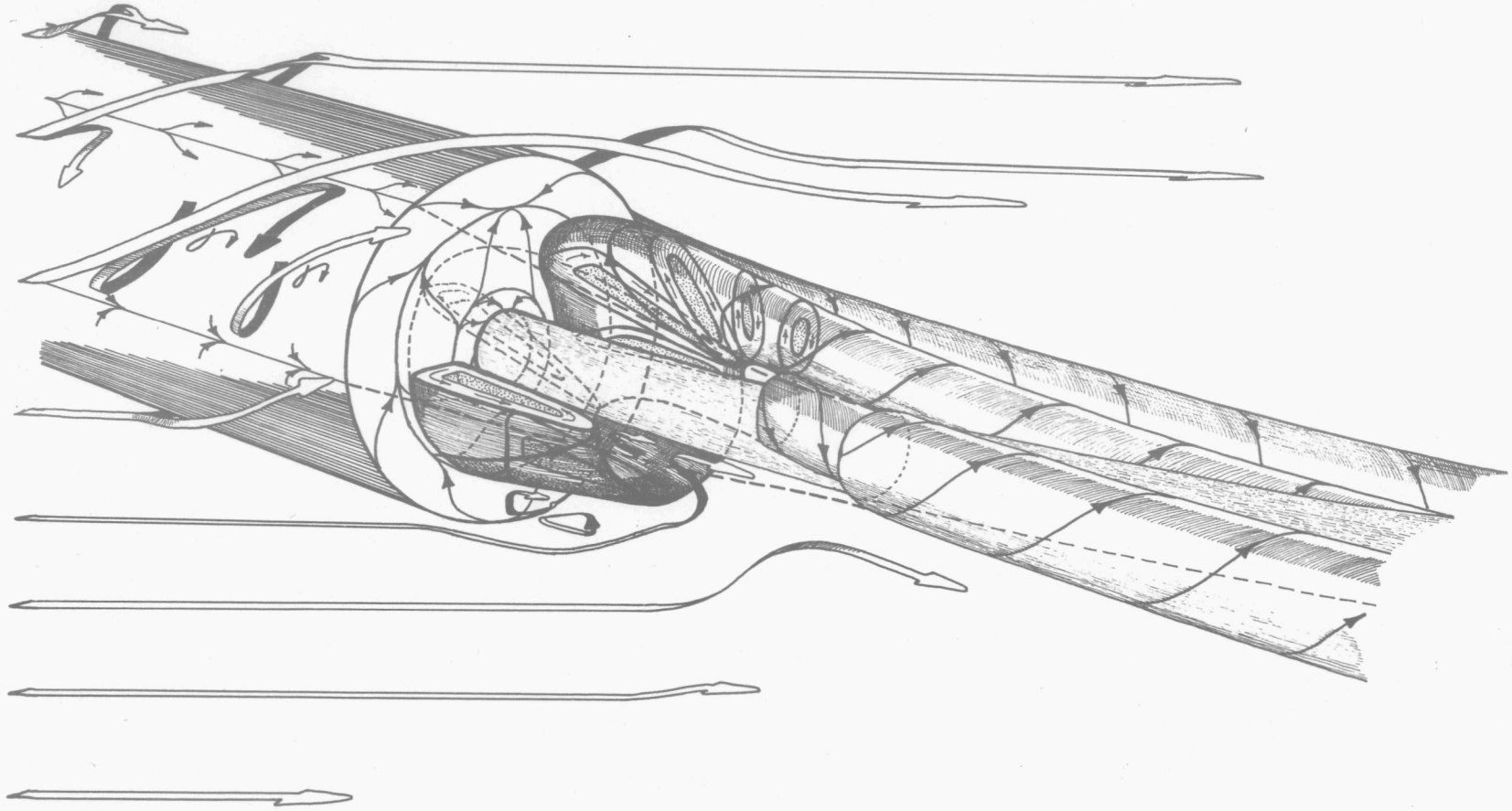

FIG. 16. THE FLOW IN THE MIXING REGION

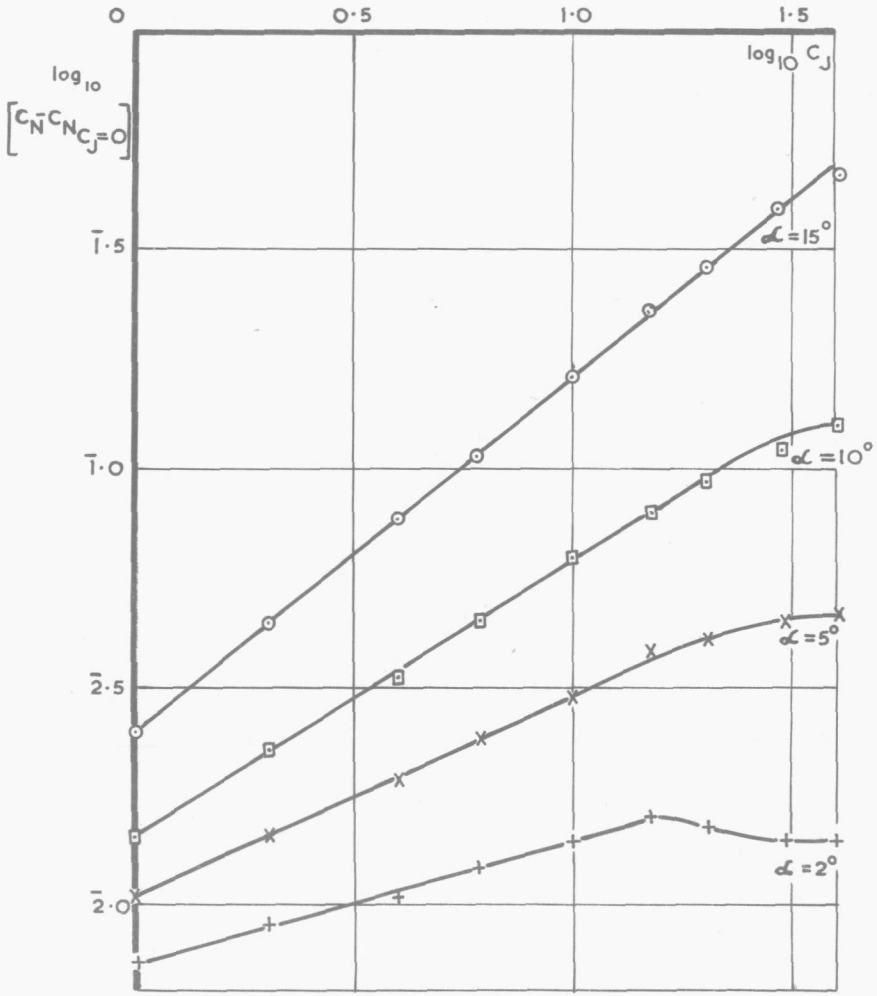

FIG. 17. DEPENDENCE OF $C_N - C_{N\,C_J=0}$ ON C_J – BLUFF AFTERBODY

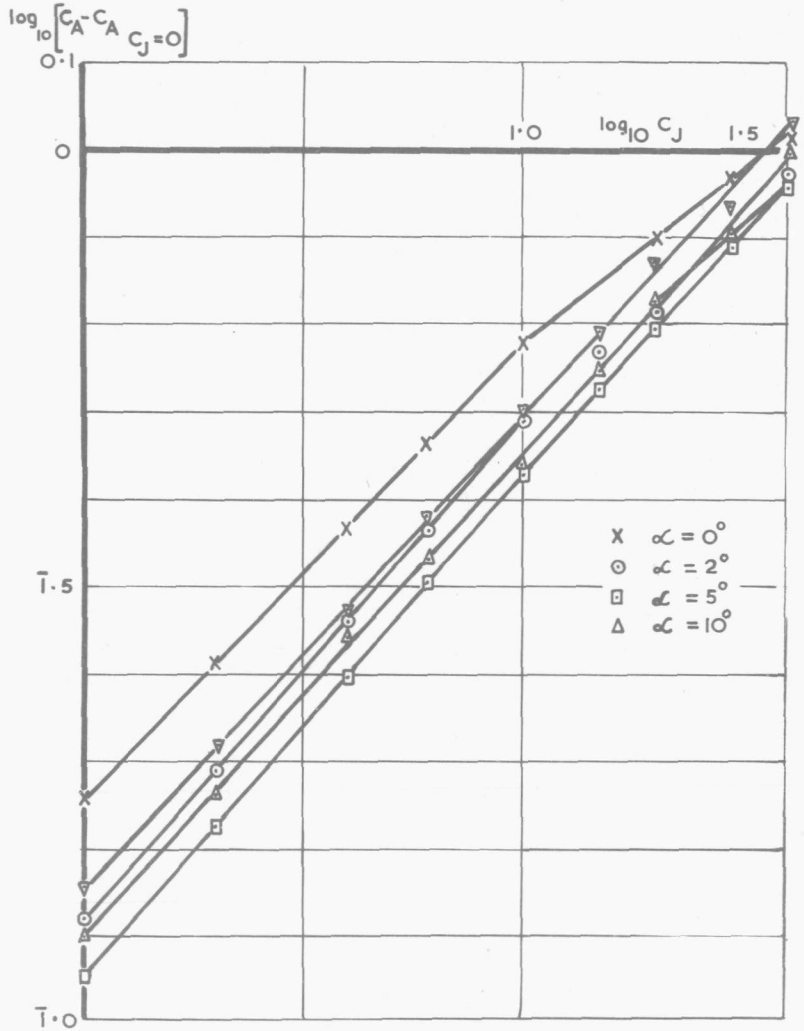

FIG. 18. DEPENDENCE OF $C_A - C_{A\,C_J=0}$ ON C_J – BLUFF AFTERBODY